









Kilonova and Optical Afterglow from Binary Neutron Star Mergers. II. Optimal Search Strategy for Serendipitous Observations and Target-of-opportunity Observations of Gravitational-wave Triggers

JIN-PING ZHU ¹, SHICHAO WU ^{2,3}, YUAN-PEI YANG ⁴, BING ZHANG ⁵, HAO-RAN SONG ⁶, HE GAO ⁶,
ZHOUJIAN CAO ⁶, AND YUN-WEI YU ⁷

¹*Department of Astronomy, School of Physics, Peking University, Beijing 100871, China; zhujp@pku.edu.cn*

²*Max-Planck-Institut für Gravitationsphysik (Albert-Einstein-Institut), D-30167 Hannover, Germany; shichao.wu@aei.mpg.de*

³*Leibniz Universität Hannover, D-30167 Hannover, Germany*

⁴*South-Western Institute for Astronomy Research, Yunnan University, Kunming, Yunnan, People's Republic of China; ypyang@ynu.edu.cn*

⁵*Department of Physics and Astronomy, University of Nevada, Las Vegas, NV 89154, USA; bing.zhang@unlv.edu*

⁶*Department of Astronomy, Beijing Normal University, Beijing 100875, China*

⁷*Institute of Astrophysics, Central China Normal University, Wuhan 430079, China*

ABSTRACT

In the second work of this series, we explore the optimal search strategy for serendipitous and gravitational-wave-triggered target-of-opportunity observations of kilonovae and optical short-duration gamma-ray burst (sGRB) afterglows from binary neutron star (BNS) mergers, assuming that cosmological kilonovae are AT2017gfo-like (but with viewing-angle dependence) and that the properties of afterglows are consistent with those of cosmological sGRB afterglows. A one-day cadence serendipitous search strategy with an exposure time of ~ 30 s can always achieve an optimal search strategy of kilonovae and afterglows for various survey projects. We show that the optimal detection rates of the kilonova-dominated (afterglow-dominated) events are $\sim 0.2/0.5/0.8/20 \text{ yr}^{-1}$ ($\sim 500/300/600/3000 \text{ yr}^{-1}$) for ZTF/Mephisto/WFST/LSST, respectively. A better search strategy for SiTian is to increase the exposure time. SiTian can find $\sim 5(6000) \text{ yr}^{-1}$ kilonova-dominated (afterglow-dominated) events. We predict abundant off-axis orphan afterglows may be recorded in the survey database although not been identified. For target-of-opportunity observations, we simulate the maximum BNS gravitational-wave (GW) detection rates, which are $\sim 27/210/1800/2.0 \times 10^5 \text{ yr}^{-1}$, in the networks of 2nd/2.5th/3rd(Voyager)/3rd(ET&CE)-generation GW detectors. In the upcoming 2nd-generation networks, follow-up observations with a limiting magnitude of $m_{\text{limit}} \gtrsim 22 - 23 \text{ mag}$ can discover all EM signals from BNS GW events. Among these detected GW events, $\sim 60\%$ events ($\sim 16 \text{ yr}^{-1}$) can detect clear kilonova signals, while afterglow-dominated events would account for the other $\sim 40\%$ events ($\sim 11 \text{ yr}^{-1}$). In the 2.5th- and 3rd(Voyager)-generation era, the critical magnitudes for the detection of EM emissions from all BNS GW events would be $\sim 23.5 \text{ mag}$ and $\sim 25 \text{ mag}$, respectively. Foreseeable optical survey projects cannot detect all EM signals of GW events detected during the ET&CE era.

Keywords: Gravitational waves (678), Neutron stars (1108), Gamma-ray bursts (629)

1. INTRODUCTION

Kilonovae (Li & Paczyński 1998; Metzger et al. 2010) and short-duration gamma-ray bursts (sGRB; Paczynski 1986, 1991; Eichler et al. 1989; Narayan et al. 1992; Zhang 2018) have long been thought to originate from binary neutron star (BNS) and neutron star–black hole (NSBH) mergers. The interaction of the sGRB relativistic jets with the surrounding interstellar medium would

produce bright afterglow emissions from X-ray to radio¹ (Rees & Meszaros 1992; Meszaros & Rees 1993; Paczyn-

¹ If BNS and NSBH mergers occur in active galactic nucleus (e.g., Cheng & Wang 1999; McKernan et al. 2020) accretion disks, sGRB relativistic jets would always be choked and kilonova emissions would be outshone by the disk emission (Zhu et al. 2021e; Perna et al. 2021). The choked jets and subsequent jet-cocoon and ejecta shock breakouts can generate high-energy neutrinos which may significantly contribute diffuse neutrino background (Zhu et al. 2021a,b).

ski & Rhoads 1993; Mészáros & Rees 1997; Sari et al. 1998; Gao et al. 2013b).

On 2017 August 17, the first BNS gravitational wave (GW) event, i.e., GW170817, was detected by the Advanced Laser Interferometer Gravitational Wave Observatory (LIGO; Harry & LIGO Scientific Collaboration 2010; LIGO Scientific Collaboration et al. 2015) and the Advanced Virgo (Acernese et al. 2015) detectors (Abbott et al. 2017a). This BNS GW event has been subsequently confirmed in connection with an sGRB (GRB170817A; Abbott et al. 2017b; Goldstein et al. 2017; Savchenko et al. 2017; Zhang et al. 2018a), an ultraviolet–optical–infrared kilonova (AT2017gfo; Abbott et al. 2017c; Andreoni et al. 2017; Arcavi et al. 2017; Chornock et al. 2017; Coulter et al. 2017; Covino et al. 2017; Cowperthwaite et al. 2017; Díaz et al. 2017; Drout et al. 2017; Evans et al. 2017; Hu et al. 2017; Kasliwal et al. 2017; Kilpatrick et al. 2017; Lipunov et al. 2017; McCully et al. 2017; Nicholl et al. 2017; Pian et al. 2017; Shappee et al. 2017; Smartt et al. 2017; Soares-Santos et al. 2017; Tanvir et al. 2017; Utsumi et al. 2017; Valenti et al. 2017; Villar et al. 2017) and a broadband off-axis jet afterglow (Alexander et al. 2017; Haggard et al. 2017; Hallinan et al. 2017; Margutti et al. 2017; Troja et al. 2017, 2018, 2020; D’Avanzo et al. 2018; Dobie et al. 2018; Lazzati et al. 2018; Lyman et al. 2018; Xie et al. 2018; Piro et al. 2019; Ghirlanda et al. 2019). The multi-messenger observations of this BNS merger provided smoking-gun evidence for the long-hypothesized origin of sGRBs and kilonovae, and heralded the advent of the GW-led astronomy era.

To date, except for AT2017gfo, other kilonova candidates were all detected in superposition with decaying sGRB afterglows (e.g., Berger et al. 2013; Tanvir et al. 2013; Fan et al. 2013; Gao et al. 2015, 2017; Jin et al. 2015, 2016, 2020; Yang et al. 2015; Gompertz et al. 2018; Ascenzi et al. 2019; Rossi et al. 2020; Ma et al. 2021; Fong et al. 2021; Wu et al. 2021; Yuan et al. 2021). One possible reason is that most BNS and NSBH mergers are far away from us. Their associated kilonova signals may be too faint to be directly detected by present survey projects. However, thanks to the beaming effect of relativistic jets, in Paper I of this series (Zhu et al. 2021d), we have shown that a large fraction of cosmological afterglows could be much brighter than the associated kilonovae if the jets move towards or close to the line of sight. Bright afterglow emissions would help us detect potential associated kilonova emissions. On the other hand, a too bright afterglow would also affect on the detectability of the associated kilonova.

Catching more kilonovae and afterglows by current and future survey projects would expand our knowl-

edge about the population properties of these events. Kasliwal et al. (2020); Mohite et al. (2021) constrained the population properties of kilonovae based on the non-detection of GW-triggered follow-up observations during O3. Although the properties of kilonova and afterglow emissions from BNS and NSBH mergers can be reasonably well predicted, their low luminosities and fast evolution nature compared with supernova emission makes it difficult to detect them using the traditional time-domain survey projects. Several works in the literature have studied the detection rates and search strategy for kilonovae by serendipitous observations (e.g., Metzger & Berger 2012; Coughlin et al. 2017, 2020a; Rosswog et al. 2017; Scolnic et al. 2018; Setzer et al. 2019; Sagués Carracedo et al. 2021; Zhu et al. 2021e; Andreoni et al. 2021a; Almualla et al. 2021; Chase et al. 2021). Because afterglow emission could significantly affect the observation of a large fraction of kilonova events, one cannot ignore the effect of afterglow emission when considering the research strategy and detectability of kilonova emission. In the second work of this series, we will perform a detailed study on optimizing serendipitous detections of both kilonovae and optical afterglows with different cadences, filters, and exposure times for several present and future survey projects. The survey projects we consider in this work include the Zwicky Transient Facility (ZTF; Bellm et al. 2019; Masci et al. 2019), the Multi-channel Photometric Survey Telescope² (Mephisto; Er et al. 2021, in preparation), the Wide Field Survey Telescope (WFST; et al. Kong et al. 2021, in preparation), the Large Synoptic Survey Telescope (LSST; LSST Science Collaboration et al. 2009), and the SiTian Projects (SiTian; Liu et al. 2021). We note that NSBH mergers may have a lower event rate density, that NSBH kilonovae may be dimmer than BNS kilonovae (e.g., Zhu et al. 2020) and that most NSBH mergers in the universe are likely plunging events (e.g., Abbott et al. 2021a; Zappa et al. 2019; Drozda et al. 2020; Zhu et al. 2021c; Broekgaarden et al. 2021). As a result, the detection rates of kilonova and afterglow emissions from NSBH mergers should be much lower than those from BNS mergers (Zhu et al. 2021f). In the following calculations, we only consider kilonova and afterglow emissions from BNS mergers.

Furthermore, with the upgrade and iteration of GW observatories, numerous BNS mergers from the distant universe will be discovered. Future foreseeable GW observations will give a better constraint on the localization for a fraction of BNS GW events, which will benefit

² <http://www.mephisto.ynu.edu.cn/site/>

the search for associated electromagnetic (EM) counterparts. For example, some GW sources will be localized to $\sim 10 \text{ deg}^2$ by the network including the Advanced LIGO, Advanced Virgo, and KAGRA GW detectors (Abbott et al. 2020; Frostig et al. 2021). Therefore, taking advantage of target-of-opportunity (ToO) follow-up observations of GW triggers will greatly improve the search efficiency of kilonovae and afterglows. The kilonova follow-up campaigns by specific survey projects, e.g., ZTF, LSST, and the Wide-Field Infrared Transient Explorer, for GW BNS mergers in the near GW era have been simulated recently (Sagués Carracedo et al. 2021; Cowperthwaite et al. 2019; Frostig et al. 2021). In this paper, we present detailed calculations of the BNS detectability by the GW detectors in the next 15 yr and the associated EM detectability for GW-triggered ToO observations.

The paper is organized as follows. The physical models are briefly presented in Section 2. More details of our models have been presented in Paper I. The search strategy and detectability of kilonova and afterglow emissions for time-domain survey observations is studied in Section 3. We also perform calculations of EM detection rates for some specific survey projects. In Section 4, we simulate the GW detection and subsequent detectability of EM ToO follow up observations for networks of 2nd-, 2.5th-, and 3rd-generation GW detectors. Finally, we summarize our conclusions and present some discussion in Section 5. A standard Λ CDM cosmology with $H_0 = 67.8 \text{ km s}^{-1} \text{ Mpc}^{-1}$, $\Omega_\Lambda = 0.692$, and $\Omega_m = 0.308$ (Planck Collaboration et al. 2016) is applied in this paper.

2. MODELLING

In this section, we only briefly introduce our model. The modeling details of redshift distribution, jet afterglow and kilonova emissions of BNS mergers has been presented in Paper I.

The total number of BNS mergers in the universe can be estimated as (e.g., Sun et al. 2015)

$$\dot{N}_{\text{BNS}} \approx \int_0^{z_{\text{max}}} \frac{\dot{\rho}_{0,\text{BNS}} f(z)}{1+z} \frac{dV(z)}{dz} dz, \quad (1)$$

where $\dot{\rho}_{0,\text{BNS}}$ is the local BNS event rate density, $f(z)$ is the dimensionless redshift distribution factor, and z_{max} is the maximum redshift for BNS mergers. The comoving volume element $dV(z)/dz$ in Equation (1) is

$$\frac{dV}{dz} = \frac{c}{H_0} \frac{4\pi D_L^2}{(1+z)^2 \sqrt{\Omega_\Lambda + \Omega_m(1+z)^3}}, \quad (2)$$

where c is the speed of light and D_L is the luminosity distance, which is expressed as

$$D_L = (1+z) \frac{c}{H_0} \int_0^z \frac{dz}{\sqrt{\Omega_\Lambda + \Omega_m(1+z)^3}} \quad (3)$$

Recently, Abbott et al. (2021b) estimated the local BNS event rate density as $\dot{\rho}_{0,\text{BNS}} = 320_{-240}^{+490} \text{ Gpc}^{-3} \text{ yr}^{-1}$ based on the GW observations during the first half of the third observing (O3) run (see Mandel & Broekgaarden 2021, for a review of $\dot{\rho}_{0,\text{BNS}}$). Hereafter, if not otherwise specified, $\dot{\rho}_{0,\text{BNS}}$ used in our calculations are simply set as the median value of the GW constraint by the LIGO/Virgo Collaboration (LVC), i.e., $\dot{\rho}_{0,\text{BNS}} \simeq 320 \text{ Gpc}^{-3} \text{ yr}^{-1}$.

BNS mergers can be thought as occurring with a delay timescale with respect to the star formation history. The Gaussian delay model (Virgili et al. 2011), log-normal delay model (Wanderman & Piran 2015), and power-law delay model (Virgili et al. 2011) are main types of delay time distributions. Among these three delay models, the log-normal delay model is one of the favored one to explain the observations of sGRBs (Sun et al. 2015). We therefore only adopt the log-normal delay model as our merger delay model and the analytical fitting expression of $f(z)$ is presented as Equation (A8) in Zhu et al. (2021f). With known redshift distribution $f(z)$, we randomly simulate a group of $n_{\text{sim}} = 5 \times 10^6$ BNS events in the universe based on Equation (1).

For each BNS event, we then generate its EM emissions. We briefly assume that all of BNS events in the universe would only power three main types of EM signals, i.e. the sGRB, the jet afterglow, and the kilonova. We note that sGRBs are only used in the discussion of GW-triggered ToO observations in Section 4. Our viewing-angle-dependent semianalytical model of sGRB emission follows Song et al. (2019) and Yu et al. (2021). The signature of sGRBs depends on the on-axis equivalent isotropic energy E_0 , the core half-opening angle θ_c , and the latitudinal viewing angle θ_{view} , while the afterglow emission has a dependence on four additional parameters, i.e. number density of interstellar medium n , power-law index of the electron distribution p , fractions of shock energy distributed in electrons, ε_e , and in magnetic fields, ε_B . Furthermore, the kilonova emission is only determined by θ_{view} . According to the distributions of above parameters as described in Paper I in detail, one can randomly generate the EM emission components for each simulated BNS event.

3. DETECTABILITY FOR SERENDIPITOUS SEARCHES

3.1. Method

Following [Zhu et al. \(2021f\)](#), we adopt a method of probabilistic statistical analysis to estimate the EM detection rate for BNS mergers. The probability that a single simulated event can be detected could be considered as the ratio of survey area within the time duration (Δt) that the brightness of the associated EM signal is above the limiting magnitude (m_{limit}) to the area of the celestial sphere ($\Omega_{\text{sph}} = 41252.96 \text{ deg}^2$). The maximum probability for a source to be detected is $\Omega_{\text{FoV}} \dot{t}_{\text{ope}} \Delta t / \Omega_{\text{sph}} (n_{\text{exp}} t_{\text{exp}} + t_{\text{oth}})$, where Ω_{FoV} is the field of view (FoV) for the specific survey project, \dot{t}_{ope} is the average operation time per day, n_{exp} is defined as the exposure number for each visit, t_{exp} is the exposure time, and t_{oth} is other time spent for each visit. However, high-cadence observations would restrict the survey area, which means that the probability of a source being detected by the high-cadence search would be a constant, i.e., $\Omega_{\text{FoV}} \dot{t}_{\text{ope}} t_{\text{cad}} / \Omega_{\text{sph}} (n_{\text{exp}} t_{\text{exp}} + t_{\text{oth}})$, where the cadence time t_{cad} defined as the interval between consecutive observations of the same sky area by a telescope. Furthermore, the event should appear in the sky coverage of the survey telescope that one can have a chance to discover it. Thus, we simply set an upper limit on the probability for a source that can be detected, which is expressed as $\Omega_{\text{cov}} / \Omega_{\text{sph}}$ with Ω_{cov} being the detectable sky coverage for a specific survey project. By counting the detection probabilities of all simulated events, one can write the EM detection rate for the serendipitous observations as

$$\dot{N}_{\text{EM}} \approx \frac{\dot{N}_{\text{BNS}}}{n_{\text{sim}}} \sum_{i=1}^{n_{\text{sim}}} \min \left[\frac{\Omega_{\text{cov}}}{\Omega_{\text{sph}}}, \frac{\Omega_{\text{FoV}} \dot{t}_{\text{ope}} \min(t_{\text{cad}}, \Delta t_i)}{\Omega_{\text{sph}} (n_{\text{exp}} t_{\text{exp}} + t_{\text{oth}})} \right], \quad (4)$$

We roughly assume that the average operation time per day is $\dot{t}_{\text{ope}} \approx 6 \text{ hr day}^{-1}$ for all survey projects except for SiTian. The time spent for each visit t_{oth} is dependent on the technical performance of specific survey project and different search strategy. Because t_{oth} is uncertain, we set it as a constant for each survey project, i.e., $t_{\text{oth}} = 15 \text{ s}$.

In order to reject the supernova background and other rapid-evolving transients, in [Paper I](#), we showed that one can use the unique color evolution of kilonovae and afterglows to identify them among the observed transients. We require that the judgement condition for the detection of the kilonova and/or afterglow by a serendipitous search is that “two different exposure filters have at least two detection epochs”. It would be $n_{\text{exp}} = 1$ for Mephisto and SiTian since these two survey projects can achieve simultaneous imaging in three bands, while $n_{\text{exp}} = 2$ for ZTF, WFST, and LSST.

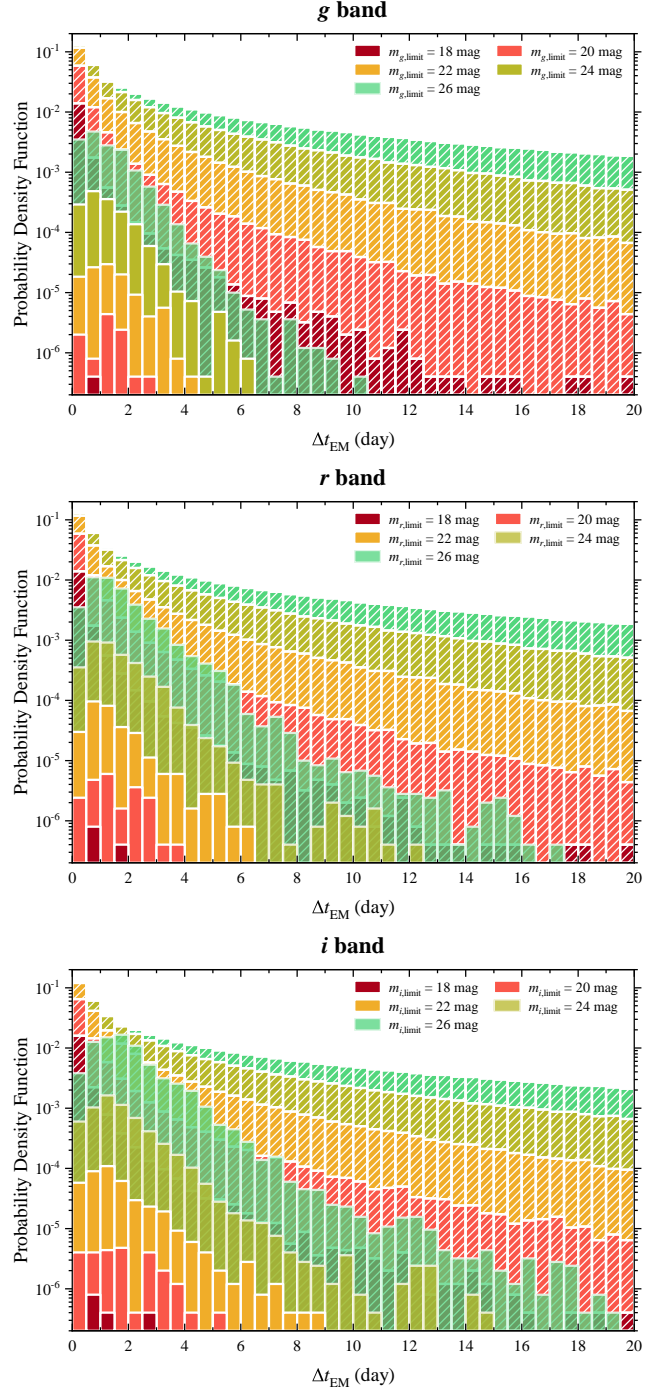


Figure 1. Crimson, red, orange, yellowgreen, and green histograms are the probability density functions of Δt_{KN} (solid histograms) and Δt_{AG} (striped histograms) for a limiting magnitude of $m_{\text{limit}} = 18, 20, 22, 24$, and 26 , in g band (top panel), r band (medium panel), and i band (bottom panel). The bin width of the histograms is set as $\Delta = 0.5 \text{ d}$.

3.2. Δt_{EM} and Cadence Time Selection

As listed in [Table 1](#), we show the 90% credible regions of two timescales, i.e., Δt_{KN} and Δt_{AG} , with different

Table 1. Time during which the brightness of EM counterpart is above the limiting magnitude

Filter	Parameter	$m_{\text{limit}} = 18 \text{ mag}$	19 mag	20 mag	21 mag	22 mag	23 mag	24 mag	25 mag	26 mag
<i>u</i>	Δt_{KN}	—	$0.67^{+0}_{-0.67}$	$0.65^{+0.77}_{-0.65}$	$0.82^{+0.63}_{-0.72}$	$0.8^{+1.1}_{-0.6}$	$0.7^{+1.4}_{-0.6}$	$0.7^{+1.3}_{-0.5}$	$0.7^{+1.2}_{-0.6}$	$0.8^{+1.2}_{-0.6}$
	Δt_{AG}	$0.2^{+1.1}_{-0.1}$	$0.2^{+1.4}_{-0.2}$	$0.3^{+2.0}_{-0.2}$	$0.3^{+3.0}_{-0.3}$	$0.4^{+4.7}_{-0.4}$	$0.6^{+7.8}_{-0.5}$	1^{+13}_{-1}	1^{+19}_{-1}	2^{+18}_{-2}
<i>g</i>	Δt_{KN}	$0.83^{+0}_{-0.83}$	$0.7^{+1.1}_{-0.7}$	$1.3^{+0.8}_{-1.2}$	$1.2^{+1.4}_{-1.0}$	$1.2^{+1.9}_{-0.9}$	$1.1^{+1.7}_{-0.8}$	$1.0^{+1.7}_{-0.7}$	$0.9^{+1.8}_{-0.7}$	$0.9^{+1.9}_{-0.7}$
	Δt_{AG}	$0.2^{+1.2}_{-0.2}$	$0.2^{+1.6}_{-0.2}$	$0.3^{+2.2}_{-0.2}$	$0.3^{+3.3}_{-0.3}$	$0.4^{+5.2}_{-0.4}$	$0.6^{+8.7}_{-0.6}$	1^{+15}_{-1}	2^{+18}_{-1}	3^{+17}_{-3}
<i>v</i>	Δt_{KN}	$1.4^{+0}_{-1.4}$	$0.7^{+1.1}_{-0.6}$	$1.1^{+1.5}_{-0.8}$	$1.0^{+2.4}_{-0.8}$	$1.1^{+2.3}_{-0.7}$	$1.0^{+2.0}_{-0.8}$	$1.1^{+1.9}_{-0.8}$	$1.2^{+2.0}_{-0.9}$	$1.3^{+1.9}_{-0.7}$
	Δt_{AG}	$0.2^{+1.3}_{-0.2}$	$0.2^{+1.7}_{-0.2}$	$0.3^{+2.3}_{-0.3}$	$0.3^{+3.5}_{-0.3}$	$0.5^{+5.5}_{-0.4}$	$0.6^{+9.2}_{-0.6}$	1^{+15}_{-1}	2^{+18}_{-2}	3^{+17}_{-3}
<i>w</i>	Δt_{KN}	$0.5^{+1.1}_{-0.5}$	$0.89^{+0.88}_{-0.60}$	$1.2^{+1.6}_{-0.9}$	$1.2^{+2.3}_{-0.8}$	$1.2^{+2.3}_{-0.8}$	$1.1^{+2.3}_{-0.8}$	$1.1^{+2.2}_{-0.8}$	$1.2^{+2.1}_{-0.8}$	$1.3^{+2.0}_{-1.0}$
	Δt_{AG}	$0.2^{+1.3}_{-0.2}$	$0.2^{+1.7}_{-0.2}$	$0.3^{+2.4}_{-0.3}$	$0.3^{+3.6}_{-0.3}$	$0.5^{+5.7}_{-0.4}$	$0.6^{+9.4}_{-0.6}$	1^{+16}_{-1}	2^{+18}_{-2}	3^{+17}_{-3}
<i>r</i>	Δt_{KN}	$0.7^{+1.0}_{-0.7}$	$1.07^{+0.88}_{-0.69}$	$1.3^{+1.7}_{-1.0}$	$1.2^{+2.5}_{-0.8}$	$1.1^{+2.4}_{-0.8}$	$1.3^{+2.1}_{-0.9}$	$1.3^{+2.2}_{-0.9}$	$1.2^{+2.4}_{-0.9}$	$1.3^{+2.4}_{-0.9}$
	Δt_{AG}	$0.2^{+1.4}_{-0.2}$	$0.2^{+1.7}_{-0.2}$	$0.3^{+2.4}_{-0.3}$	$0.4^{+3.6}_{-0.3}$	$0.5^{+5.8}_{-0.4}$	$0.7^{+9.6}_{-0.6}$	1^{+16}_{-1}	2^{+18}_{-2}	3^{+17}_{-3}
<i>i</i>	Δt_{KN}	$0.7^{+1.9}_{-0.7}$	$1.3^{+1.3}_{-0.7}$	$1.5^{+2.2}_{-1.3}$	$1.4^{+3.1}_{-0.9}$	$1.3^{+2.6}_{-1.0}$	$1.3^{+2.4}_{-1.0}$	$1.4^{+2.4}_{-0.9}$	$1.4^{+2.5}_{-1.0}$	$1.7^{+2.6}_{-1.2}$
	Δt_{AG}	$0.2^{+1.5}_{-0.2}$	$0.2^{+1.9}_{-0.2}$	$0.3^{+2.6}_{-0.3}$	$0.4^{+3.9}_{-0.3}$	$0.5^{+6.2}_{-0.4}$	$0.7^{+9.6}_{-0.6}$	1^{+17}_{-1}	2^{+18}_{-2}	3^{+17}_{-3}
<i>z</i>	Δt_{KN}	$0.8^{+2.3}_{-0.8}$	$1.6^{+1.6}_{-1.1}$	$2.0^{+2.3}_{-1.4}$	$1.8^{+3.0}_{-1.3}$	$1.8^{+2.7}_{-1.3}$	$1.8^{+2.6}_{-1.3}$	$1.6^{+2.9}_{-1.1}$	$1.6^{+3.1}_{-1.2}$	$1.7^{+2.8}_{-1.3}$
	Δt_{AG}	$0.2^{+1.5}_{-0.2}$	$0.2^{+2.0}_{-0.2}$	$0.3^{+2.8}_{-0.3}$	$0.4^{+4.2}_{-0.4}$	$0.5^{+6.7}_{-0.5}$	1^{+11}_{-1}	1^{+19}_{-1}	2^{+18}_{-2}	3^{+17}_{-3}
<i>y</i>	Δt_{KN}	$1.0^{+2.2}_{-1.0}$	$1.8^{+1.5}_{-1.7}$	$2.1^{+2.2}_{-1.7}$	$1.8^{+3.6}_{-1.4}$	$1.9^{+2.9}_{-1.4}$	$1.9^{+2.7}_{-1.4}$	$1.9^{+2.9}_{-1.4}$	$1.9^{+2.8}_{-1.5}$	$1.7^{+3.2}_{-1.4}$
	Δt_{AG}	$0.2^{+1.6}_{-0.2}$	$0.2^{+2.1}_{-0.2}$	$0.3^{+2.9}_{-0.3}$	$0.4^{+4.4}_{-0.4}$	$0.5^{+7.0}_{-0.5}$	1^{+12}_{-1}	1^{+19}_{-1}	2^{+18}_{-2}	3^{+17}_{-3}

NOTE—The values are the timescales during which the brightness of associated kilonova (Δt_{KN}) and afterglow (Δt_{AG}) is above the 5σ limiting magnitude in different bands with 90% interval. We note that the time window of kilonova model we used (Bulla 2019; Coughlin et al. 2020b) is from 0 day to 20 day in the rest frame, so that we only calculate the lightcurves of afterglow between 0 day to 20 days. Thus, the calculated upper limit of Δt_{AG} is simply set to 20 days, which doesn't affect the final results of EM detection rates.

filters and different limiting magnitudes. These two parameters are respectively defined as the timescales during which the brightness of the associated kilonova and afterglow is above the limiting magnitude in different bands. Because *gri* bands are the common filters used by various survey projects, we only show the probability density functions of Δt_{KN} and Δt_{AG} with different searching magnitudes in these three bands in Figure 1.

For $m_{\text{limit}} \leq 19 \text{ mag}$, the values of Δt_{KN} may be imprecise, due to the limited amount of the available data. One can see that the median value of Δt_{KN} is referred to lie $\sim 0.6 - 1.4 \text{ day}$ in optical and $\sim 1.4 - 2.1 \text{ day}$ in infrared, which may be uncorrelated with the limiting magnitude m_{limit} . If the observer wants to achieve at least two detection epochs for at least 50% of the observable kilonova signals, the cadence time t_{cad} should be less than half of the median value of Δt_{KN} . This means t_{cad} should be $t_{\text{cad}} \lesssim 0.3 - 0.7 \text{ day}$ if one uses an optical band to search for kilonovae and $t_{\text{cad}} \lesssim 0.7 - 1.0 \text{ day}$ by an infrared band.

Unlike Δt_{KN} , there exists a positive correlation between Δt_{AG} and m_{limit} . The median value of Δt_{KN} would be always larger than Δt_{AG} if $m_{\text{limit}} \lesssim 24 \text{ mag}$. As shown in Figure 1, the probability density function of Δt_{AG} is significantly higher than that of Δt_{KN} , es-

pecially for searching with a relatively shallow limiting magnitude in a bluer filter band. Thus, it may be easier to discover optical afterglows by adopting the cadence of searching for kilonovae.

3.3. Optimal Search Strategy

We divide the events into two groups based on the relative brightness of the detected kilonova and afterglow. If the peak kilonova flux is five times of the afterglow flux, i.e., $F_{\nu, \text{KN}}(t_{\text{KN}, \text{p}}) > 5F_{\nu, \text{AG}}(t_{\text{KN}, \text{p}})$, where $t_{\text{KN}, \text{p}}$ is the peak time of the kilonova, we qualify these events into “kilonova-dominated sample”. For such events, kilonova emission at the peak time would be at least two magnitudes brighter than that of the associated afterglow emission, so that this requirement can guarantee a clear kilonova signal for observers. Other events are classified as “afterglow-dominated sample”, since the observed kilonova signals of these events may be ambiguous. Values of some technical parameters, including the expected limiting magnitude which is a logarithmic function of exposure time in each band, FoV, detectable sky coverage, for the survey telescopes we considered are presented in Table 2. We respectively show the detection rates of kilonova-dominated and afterglow-dominated sample for ZTF, Mephisto, WFST, and LSST in Fig-

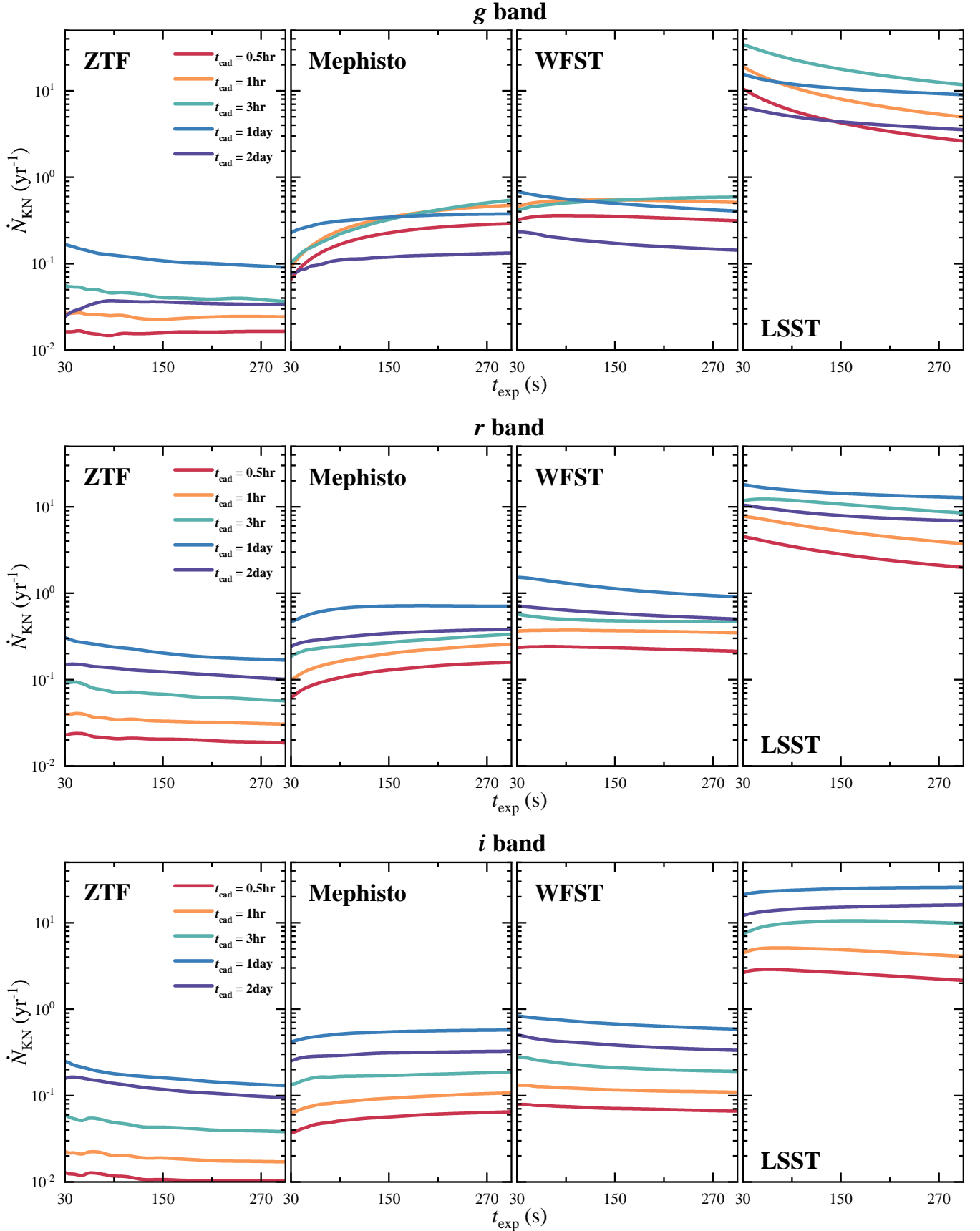


Figure 2. Detection rates of kilonova-dominated sample as functions of exposure time t_{exp} and cadence time t_{cad} for serendipitous observations. Four survey projects, including ZTF, Mephisto, WFST, and LSST (from left to right panels), are considered. The panels from top to bottom represent events of kilonova-dominated sample to be detected in the g band, r band, and i band, respectively. Red, orange, green, blue, and violet lines are the detection rates by adopting cadence searching strategies of $t_{\text{cad}} = 0.5 \text{ hr}$, 1 hr , 3 hr , 1 day , and 2 day , respectively.

Table 2. Summary Technical Information for Each Survey

Telescope	$m_{\text{limit}} = a \times t_{\text{exp}}^b$						FoV/deg ²	Sky Coverage/deg ²	Reference
ZTF	<i>g</i>		<i>r</i>		<i>i</i>		47.7	30,000	(1)
	18.62		18.37		17.91				
	0.026		0.026		0.027				
Mephisto	<i>u</i>	<i>v</i>	<i>g</i>	<i>r</i>	<i>i</i>	<i>z</i>	3.14	26,000	(2)
	18.45	18.54	19.91	19.91	19.68	18.71			
	0.043	0.042	0.034	0.032	0.030	0.033			
WFST	<i>u</i>	<i>g</i>	<i>r</i>	<i>i</i>	<i>z</i>	<i>w</i>	6.55	20,000	(3)
	20.70	21.33	21.13	20.46	19.41	21.33			
	0.022	0.022	0.022	0.023	0.024	0.022			
LSST	<i>u</i>	<i>g</i>	<i>r</i>	<i>i</i>	<i>z</i>	<i>y</i>	9.6	20,000	(4)
	22.03	23.60	22.54	21.73	21.83	21.68			
	0.025	0.018	0.023	0.030	0.031	0.032			
SiTian *	<i>g</i>		<i>r</i>		<i>i</i>		600	30,000	(5)
	18.62		18.37		17.91				
	0.026		0.026		0.027				

NOTE—The columns are [1] the survey project; [2] the search limiting magnitude m_{limit} as a logarithmic function of exposure time t_{exp} in different bands for specific survey project (parameter a and b are respectively the values at the second and third sub-rows of each row); [3] field of view Ω_{FoV} ; [4] detectable sky coverage Ω_{cov} ; [5] references.

Reference: (1) [Bellm et al. \(2019\)](#); [Masci et al. \(2019\)](#); (2) [Er et al. \(2021\)](#), in preparation; [Lei et al. \(2021\)](#) (3) [Kong et al. \(2021\)](#), in preparation; [Shi et al. \(2018\)](#) (4) [LSST Science Collaboration et al. \(2009\)](#); (5) [Liu et al. \(2021\)](#).

* The technical specification of the limiting magnitude in the g -band stacked images for SiTian is similar to that for ZTF ([Liu et al. 2021](#)). SiTian would simultaneously observe the same visit in three different filters (u , g , i). Due to the lack of the technical information in u and i band of SiTian, we simply use the technical information of ZTF in gri bands to calculate the EM detection rates by SiTian.

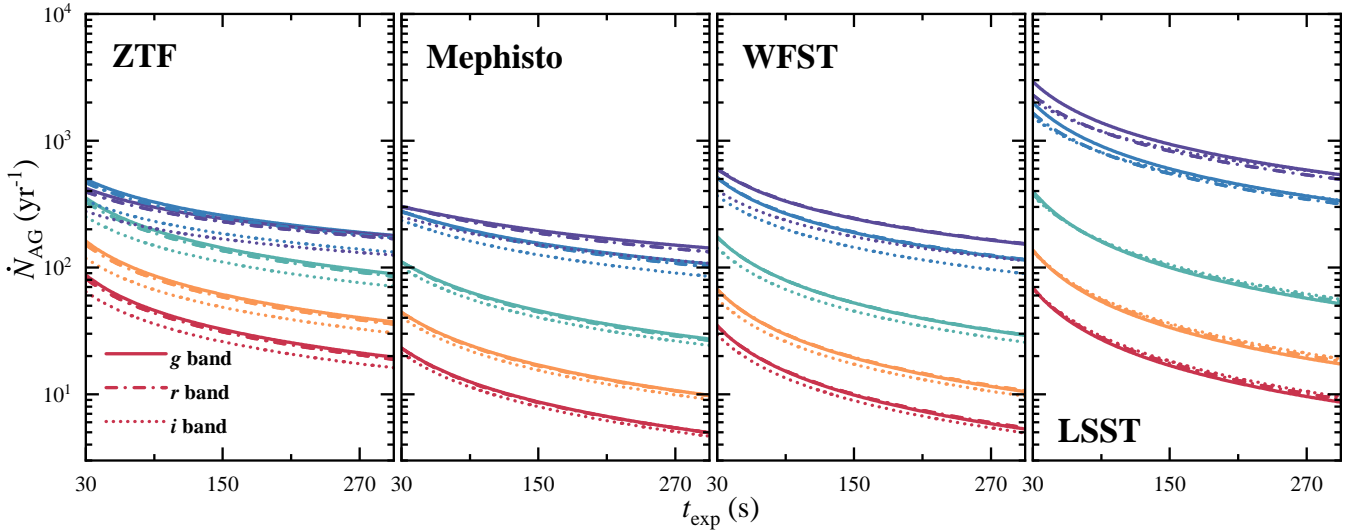


Figure 3. Similar to Figure 2, but for the detection rates of afterglow-dominated sample. Solid, dashed-dotted, and dotted lines represent the detection rates in g , r , and i band, respectively.

ure 2 and Figure 3, by considering exposure time from 30 s to 300 s and five different cadence timescales $t_{\text{cad}} = 0.5 \text{ hr}, 1 \text{ hr}, 3 \text{ hr}, 1 \text{ day}, \text{ and } 2 \text{ day}$. The results shown in Figure 2 and Figure 3 are only considered in *gri* bands since these three bands are commonly used bands for these survey telescopes. Because SiTian is an integrated network of dozens of survey and follow-up telescopes, its survey strategy should have a large difference with that of other survey projects. We will give an separate calculation of EM detection rates for SiTian in Section 3.4.

As shown in Figure 2, for each survey project, the difference of the detection rate for kilonova-dominated events between different bands seems very small, which is a factor of the order of unity. Kilonova detection rates by using a three-hour cadence in *g* band for Mephisto, WFST and LSST are sometimes slightly higher than those by using the one-day cadence strategy. For other cases, an one-day cadence strategy can always discover the highest number of kilonovae. As for ZTF, WFST, and LSST, kilonova detection rates would decline as the exposure time increases. On the contrary, a longer exposure time can discover more kilonova events for Mephisto. Simultaneous imaging in three bands by Mephisto is the reason for the difference of the detection rates between Mephisto and other survey projects. However, the increase in the amount of discovered kilonovae with longer exposure times is not significant. To sum up, an one-day cadence strategy with a $\sim 30 \text{ s}$ exposure time is recommended to achieve optimal search for kilonovae. The maximum kilonova detection rates for ZTF, Mephisto, WFST, and LSST are $\sim 0.2 \text{ yr}^{-1}$, $\sim 0.5 \text{ yr}^{-1}$, $\sim 0.8 \text{ yr}^{-1}$, and 20 yr^{-1} , respectively.

For afterglow-dominated events, there is no significant difference between searching in the optical and in the infrared bands for each survey project. The detection rates would drop with the increase of the exposure time. By adopting the optimal search strategy for kilonovae, one can also discover many afterglows from BNS mergers whose detection rate is much higher than that of kilonovae. For this case, the afterglow detection rates for ZTF, Mephisto, WFST, and LSST are $\sim 500 \text{ yr}^{-1}$, $\sim 300 \text{ yr}^{-1}$, $\sim 600 \text{ yr}^{-1}$, and 3000 yr^{-1} , respectively.

3.4. Optimal Search Strategy for SiTian

SiTian (Liu et al. 2021) is composed of a number of “units” deployed partly in China and partly at various sites around the world. Each unit includes three 1-m-class Schmidt telescopes with a FoV of $\Omega_{\text{FoV}} = 25 \text{ deg}^2$, which will simultaneously observe the same visit in three different optical filters. There will be also three or four 4-m-class telescopes for spectral identification and follow-up studies within the project.

SiTian planed to scan at least $10,000 \text{ deg}^2$ of sky every 30 min, down to a detection limit of $g \approx 21 \text{ mag}$ with an exposure time of $\sim 1 \text{ min}$ using at least 14 units in China. Furthermore, at least 10 units outside China can survey an additional $\sim 20,000 \text{ deg}^2$ with a slightly lower cadence (a few hr). Based on this fiducial search plan of SiTian, we change the cadence time and exposure time for all of units to explore the optical search strategy of SiTian, while preserving the same sky coverage.

The results of EM detection rates for SiTian are shown in Table 3. We show that SiTian can detect $\sim 6 \times 10^3 \text{ yr}^{-1}$ afterglow-dominated events. The detection rate of kilonova-dominated events is $\sim (1 - 2) \text{ yr}^{-1}$ by adopting the fiducial search plan of SiTian. Since kilonovae are very faint, a better search strategy would be to increase the exposure time of the telescopes with the expense of losing the cadence. The detection rate of kilonova-dominated events would slightly rise to $\sim (2 - 6) \text{ yr}^{-1}$ if an exposure time of 165 s is used.

4. DETECTABILITY FOR TARGET-OF-OPPORTUNITY OBSERVATIONS OF GW TRIGGERS

4.1. GW Detectability

4.1.1. Method

It is expected that in the fourth observation run (O4) of GW detector network which will begin running in 2022, two Advanced LIGO detectors (H1 and L1) in the USA (Harry & LIGO Scientific Collaboration 2010; LIGO Scientific Collaboration et al. 2015), Advanced Virgo detector (V1) in Europe (Acernese et al. 2015), and KAGRA detector (K1) in Japan (Aso et al. 2013; Kagra Collaboration et al. 2019) will reach their respective design sensitivities (Abbott et al. 2020). The network composed of these 2nd generation detectors is referred to as the “HLVK era” in the following. The 2nd generation detectors would further be improved to 2.5th generation detectors in ~ 2025 . The subsequent upgrade of Advanced LIGO, Advanced Virgo, and KAGRA are called Advanced LIGO Plus (A+; Miller et al. 2015), Advanced Virgo Plus (AdV+; Abbott et al. 2020), and KAGRAplusCombined (KAGRA+; Michimura et al. 2020). Hereafter, we refer to the era during which these four detectors upgrade to 2.5th generation detectors as the “PlusNetwork era”. After ~ 2030 , the 3rd generation GW detectors are expected to replace the 2nd and 2.5th generation detectors. The currently proposed 3rd generation detector plans include LIGO Voyager (Adhikari et al. 2020) as an improvement upon LIGO A+, the Einstein Telescope (ET) in Europe (Punturo et al. 2010a,b; Maggiore et al. 2020), and Cosmic Explorer (CE) in the USA (Reitze et al. 2019). Due to the as-yet

Table 3. EM Detection Rates for SiTian

t_{exp}/s	$\Omega_{\text{FoV},1}/\text{deg}^2$	$t_{\text{cad},1}/\text{min}$	$\Omega_{\text{FoV},2}/\text{deg}^2$	$t_{\text{cad},2}/\text{min}$	$\dot{N}_{\text{KN}}/\text{yr}^{-1}$			$\dot{N}_{\text{AG}} \times 10^3/\text{yr}^{-1}$		
					g	r	i	g	r	i
45 (fiducial)		30		80	1.1	2.2	2.5	5.3	5.7	6.1
75	350	45	250	120	1.3	2.9	3.4	5.7	6.2	6.5
105		60		160	1.6	3.4	4.1	5.8	6.3	6.7
165		90		240	1.8	4.2	5.4	5.7	6.3	6.7

NOTE—We assume that the time between two visits is $t_{\text{oth}} = 15$ s. The operation times for units in China and outside China are assumed to be $\dot{t}_{\text{ope}} = 8 \text{ hr day}^{-1}$ and 16 hr day^{-1} , respectively. The columns are [1] the exposure time; [2] the total field of view of SiTian units in China; [3] the corresponding cadence time for SiTian units in China; [4] the total field of view of SiTian units outside China; [5] the corresponding cadence time for SiTian units outside China; [6–8] the detection rate of kilonova-dominated events in *gri* bands; [9–11] the detection rate of afterglow-dominated events in *gri* bands.

undetermined locations of ET and CE, we directly place ET at the current Virgo detector position and two CE detectors at the current H1 and V1 positions, according to the convention (Vitale & Evans 2017; Vitale & Whittle 2018).

For each BNS system, we randomly simulate the masses of individual NSs based on the observationally derived mass distribution of Galactic BNS systems, i.e., a normal distribution $M_{\text{NS}}/M_{\odot} \sim \mathcal{N}(1.32, 0.11^2)$ (Lattimer 2012; Kiziltan et al. 2013). The neutron star equation of state (EoS) DD2 (Typel et al. 2010), which is one of the stiffest EoS allowed by present constraints (e.g., Gao et al. 2016; Abbott et al. 2019), is adopted. With known M_{NS} , z , and EoS, we use the IMRPhenomPv2_NRTidalv2 (Dietrich et al. 2019) template to simulate the GW waveform in the geocentric coordinate system, and then project it to different detectors to obtain the strain signal detected by each detector. The optimal signal-to-noise ratio (S/N) can be obtained by

$$\rho_{\text{opt}}^2 = 4 \int_{f_{\text{min}}}^{f_{\text{max}}} \frac{|\tilde{h}(f)|^2}{S_n(f)} df = \int_{f_{\text{min}}}^{f_{\text{max}}} \frac{(2|\tilde{h}(f)|\sqrt{f})^2}{S_n(f)} d\ln(f), \quad (5)$$

where f is the frequency, $\tilde{h}(f)$ is the strain signal in the frequency domain, and $S_n(f)$ is the one-sided power spectral density of the GW detector which is square of the amplitude spectral density (ASD). The ASD for each detector is shown in the Appendix A. We set the maximum frequency f_{max} to 2048 Hz. The low cutoff frequency f_{min} is set to 20 Hz for O3, 10 Hz for all the 2nd, 2.5th generation detectors (Miller et al. 2015) and LIGO Voyager (Adhikari et al. 2020), 5 Hz for CE (Reitze et al. 2019), and 1 Hz for ET (Punturo et al. 2010a). We use the optimal S/N to approximate the matched filtering S/N of the GW signal detected by each detector, and then calculate the network S/N of the entire detector network, i.e., the root sum squared of the S/N of all detectors. When the S/N for a single detector is greater

than the threshold of 8 and the network S/N is greater than 12, we expect that the corresponding GW signal is detected. In order to take into account different situations in each GW era, we only calculate the worst and best cases, i.e., “only the detector with the worst sensitivity in the corresponding era works” as the worst situation and “all detectors in the corresponding era have reached the design sensitivity and work normally” as the optimal situation. During the 2nd generation detector network, the worst case is that only K1 works normally, while the best case is that H1, L1, V1, and K1 all work normally, which we abbreviate as “HLVK”. Similarly, the worst case for the 2.5th generation era is that only AdV+ works, and the best case is that A+, AdV+, and KAGRA+ all work normally, which is abbreviated as “PlusNetwork”. LIGO Voyager is separately discussed. Furthermore, a single ET is considered as the worst case while “ET&CE” represents the best case of the 3rd generation era.

Because the GWs from inspiral of BNS will reach Earth earlier than EM emission, early GW to the EM community could increase the probability of detecting early-stage EM counterparts. There has been preliminary research into early warning (e.g., Chan et al. 2018; Sachdev et al. 2020; Nitz et al. 2020; Kapadia et al. 2020; Singh et al. 2021). We will calculate the duration of BNS GW signals, which can be regarded as the upper limit of the early warning time, in different detector networks. Here we adopt the 3.5 post-Newtonian order expression for the chirp time T_{chirp} , i.e., Equation (E1) in Allen et al. (2012) to calculate the duration of the GW signal.

4.1.2. GW Detection Rates, Detectable Distance, and Signal Duration

We summarize all our simulated GW detection results of different generation eras in Table 4. The total mass, S/R, and redshift for detectable GW signals in different eras are shown in Figure 4. Except for the ET&CE era,

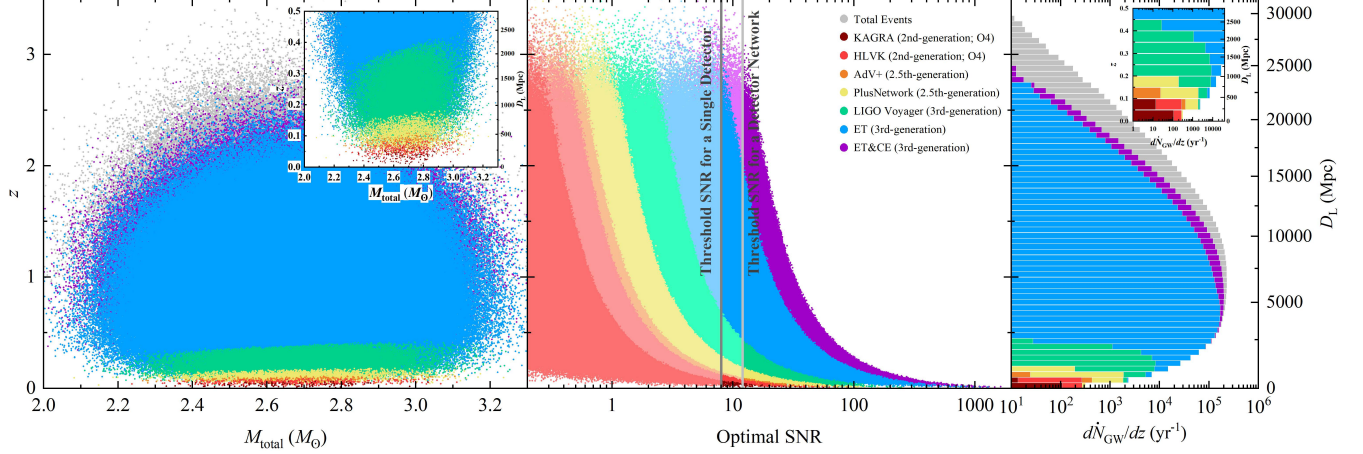


Figure 4. Detectability of BNS mergers by various detector networks in different GW detection eras. The left panels show the signals that can be detected by different detectors and detector networks. The crimson and orange dots represent the detectable signals for K1 and AdV+, while the red, yellow, green, blue, and violet dots are the GW signals detectable at HLVK, PlusNetwork, LIGO Voyager, ET, and ET&CE network eras, respectively. The gray dots in the background represent undetectable signals. The small panels in the upper right corner are enlarged images of the low-redshift area. The middle panels show the distributions of all simulated signals on the “optimal S/N-redshift” plane, with detection thresholds for a single detector (i.e., S/N = 8; gray line) and for a detector network (i.e., S/N = 12; light gray line). To the right of the thresholds are the GW signals that can be detected. The right panels show the distributions of BNS detection rates with redshift, and the insets are zoom-in pictures in the low-redshift region.

Table 4. GW Detection Results

	Era	Duty	$\dot{N}_{\text{GW}}/\text{yr}^{-1}$ ($\dot{N}_{\text{GW}}/\dot{N}_{\text{BNS}}$)	z ($D_L/100 \text{ Mpc}$)	z_{max} ($D_{L,\text{max}}/100 \text{ Mpc}$)	$T_{\text{chirp}}/\text{min}$	$(1+z)M_{\text{tot}}/M_\odot$
HLV(O3)	2nd	Network	$3.3^{+5.0}_{-2.4}$ (0.001%)	$0.025^{+0.016}_{-0.013}$ ($1.11^{+0.72}_{-0.59}$)	0.048 (2.18)	$0.97^{+0.79}_{-0.49}$	$5.1^{+2.6}_{-1.7}$
KAGRA	2nd	Single	$6.0^{+9.2}_{-4.5}$ (0.002%)	$0.035^{+0.021}_{-0.012}$ ($1.6^{+1.0}_{-1.0}$)	0.062 (2.9)	$5.6^{+4.4}_{-2.3}$	$5.4^{+2.1}_{-1.6}$
HLVK	2nd	Network	27^{+41}_{-20} (0.01%)	$0.050^{+0.028}_{-0.030}$ ($2.2^{+1.3}_{-1.4}$)	0.092 (4.3)	$6.0^{+5.8}_{-2.5}$	$5.2^{+2.0}_{-1.8}$
AdV+	2.5th	Single	34^{+53}_{-26} (0.01%)	$0.060^{+0.037}_{-0.036}$ ($2.8^{+1.8}_{-1.7}$)	0.116 (5.5)	$5.8^{+4.3}_{-2.5}$	$5.3^{+2.0}_{-1.8}$
PlusNetwork	2.5th	Network	210^{+320}_{-160} (0.08%)	$0.099^{+0.050}_{-0.055}$ ($4.7^{+2.6}_{-2.7}$)	0.190 (9.5)	$5.8^{+5.2}_{-2.4}$	$5.4^{+2.0}_{-1.7}$
LIGO Voyager	3rd	Network	$1.8^{+2.8}_{-1.4} \times 10^3$ (0.73%)	$0.22^{+0.12}_{-0.13}$ ($11.0^{+7.4}_{-6.7}$)	0.43 (24.3)	$5.8^{+4.9}_{-2.5}$	$5.3^{+2.1}_{-1.6}$
ET	3rd	Single	$1.5^{+2.3}_{-1.1} \times 10^5$ (57.0%)	$0.81^{+0.71}_{-0.47}$ (53^{+61}_{-34})	3.08 (269)	$45^{+38}_{-19} \times 60$	$5.3^{+2.1}_{-1.6}$
ET&CE	3rd	Network	$2.0^{+3.1}_{-1.5} \times 10^5$ (77.7%)	$0.91^{+0.68}_{-0.53}$ (60^{+60}_{-39})	3.34 (296)	$45^{+38}_{-19} \times 60$	$5.3^{+2.1}_{-1.6}$

NOTE—The columns are [1] the case of different generation eras; [2] the generation of GW detectors; [3] the worst case (only a single detector work) and the best case (all detector work normally) in the corresponding era; [4] median GW detection rates with consideration of 90% interval by adopting the local event rate density of $\dot{\rho}_{0,\text{BNS}} = 320^{+490}_{-240} \text{ Gpc}^{-3} \text{ yr}^{-1}$ (Abbott et al. 2021b), while the numbers in brackets are the corresponding detectable proportions of the number of BNS mergers per year in the universe (\dot{N}_{BNS}); [5] median detectable redshifts and detectable luminosities with consideration of 90% interval; [6] maximum detectable redshifts and detectable luminosities; [7] median chirp time with 90% chirp time interval; [8] median total mass in the geocentric frame with 90% interval.

the median distance of detectable GW events is always set at half of the horizon in each GW era.

We check that the maximum GW detection rate in O3 should be $\sim 3 \text{ yr}^{-1}$, which is consistent with the observations of LVC (Abbott et al. 2020, 2021c). We predict that one can detect $\sim (6-27) \text{ yr}^{-1}$ BNS GW events with a horizon at $z_{\text{max}} \sim 0.1$. For the 2.5th generation GW detector network, the detection rate is $\sim (34-210) \text{ yr}^{-1}$. The GW detection distance would be doubled compared with the detection distance in O4, i.e., the horizon can reach $z_{\text{max}} \sim 0.2$. For the LIGO Voyager in the 3rd generation era, the detection rate can be increased to $\sim 1,800 \text{ yr}^{-1}$ and the detection distance would be twice compared with the last era, i.e., a horizon of $z_{\text{max}} \sim 0.4$. However, these numbers are much smaller than those for the newly designed 3rd generation detectors. For a single ET, the detection rate is $\sim 1.5 \times 10^5 \text{ yr}^{-1}$, while for the ET&CE network, the detection rate would be $\sim 2.0 \times 10^5 \text{ yr}^{-1}$ which would account for $\sim 80\%$ of the total BNS GW events in the universe. The events detected by ET and ET&CE are mainly dominated by BNS mergers at $z \sim 1$, which is near the most probable redshift where BNS mergers occurred in the universe. The most remote detectable events by ET&CE would be at $z_{\text{max}} \sim 3.3$.

The chirp time T_{chirp} values of all the BNS signals that can be detected by each detector or detector network are shown in Figure 5. We can see a clear inversely proportional trend that the chirp time decreases as the total mass in the geocentric frame increases. In O3, the warning time of detectable BNS signals lasted for only $\sim 0.5 - 2 \text{ min}$. For the 2nd, 2.5th generations of GW detectors and LIGO Voyager, since f_{min} is reduced from 20 Hz to 10 Hz, T_{chirp} would last longer. The distributions of T_{chirp} are similar, with a median value of $\sim 6 \text{ min}$. For ET and ET&CE, f_{min} will reduce to 1 Hz, which greatly increases the signal duration. T_{chirp} has reached the order of ten hours or even a few days. There will be enough preparation times for the detection of early-stage EM emissions from BNS mergers in these cases.

4.2. EM Detectability

4.2.1. Method

The BNS GW detectabilities for the networks of 2nd, 2.5th, and 3rd generation GW detectors have been studied in detail in Section 4.1.2. Based on these results, we now discuss the EM detection probabilities for GW-triggered ToO observations under ideal follow-up conditions (i.e., the most optimal situation for detector networks of different generations).

ToO observations after GW triggers would be an optimal strategy to search for associated EM signals, mainly including sGRBs, afterglows, and kilonovae, in the future. Among these potential associated EM signals of BNS GW events, kilonovae are the most expected EM sources for astronomers to search after GW triggers. The observations of sGRBs would achieve all-sky coverage by the Gamma Ray Integrated Detectors (GRID Wen et al. 2019; Wang et al. 2021) and the Gravitational wave high-energy Electromagnetic Counterpart All-sky Monitor (GECAM; Zhang et al. 2018b; Wang et al. 2021), which can cooperate on the constraint of the sky location for BNS GW alerts. However, for on-axis or near-on-axis observers, the presence of bright jet afterglows may affect the observations of kilonovae. We grade our simulated events into four groups (“Platinum,” “Gold,” “Silver,” and “Copper”) based on the quality of kilonova observation data and localization precision of the GW event. The former three defined samples are kilonova-dominated samples while the EM signals of the Copper sample would be afterglow-dominated.

1. *Platinum.* This sample is defined by those BNS GW events that can simultaneously observe off-axis sGRBs, dim orphan afterglows, and bright kilonovae. We require the viewing angle for these events is $\theta_v > 3\theta_c$ and the kilonova flux is $F_{\nu, \text{KN}}(t_{\text{KN}, \text{p}}) > 5F_{\nu, \text{AG}}(t_{\text{KN}, \text{p}})$, which can guarantee clear kilonova signals for observers. The multi-messenger searches for GW events of this sample would be similar to the observations of GW170817/GRB170817A/AT2017gfo.

2. *Gold.* This sample include BNS GW events associated with on-axis and near-on-axis detected sGRBs. However, the brightness of afterglows for these events is too faint, so that specific kilonova signals could appear in GRB afterglows. The judgement conditions are $\theta_v < 3\theta_c$ and $F_{\nu, \text{KN}}(t_{\text{KN}, \text{p}}) > 5F_{\nu, \text{AG}}(t_{\text{KN}, \text{p}})$.

3. *Sliver.* For BNS GW events of this sample, one can detect clear kilonova signals after GW triggers. However, different from the Platinum and Gold samples, sGRB signals of GW events are too weak to trigger GRB detectors. These events could have a larger localization region due to the lack of the observations of sGRBs.

4. *Copper.* Other BNS GW events would have much brighter afterglows which could significantly affect the observations of kilonovae, i.e., $F_{\nu, \text{KN}}(t_{\text{KN}, \text{p}}) < 5F_{\nu, \text{AG}}(t_{\text{KN}, \text{p}})$. Such kilonova signals may be ambiguously recorded.

We assume that sGRBs can be triggered if $F_\gamma > F_{\gamma, \text{limit}}$, where F_γ is the γ -band flux for each BNS GW event (see Song et al. 2019; Yu et al. 2021, for the details of sGRB model) and $F_{\gamma, \text{limit}}$ is the effective sensitivity

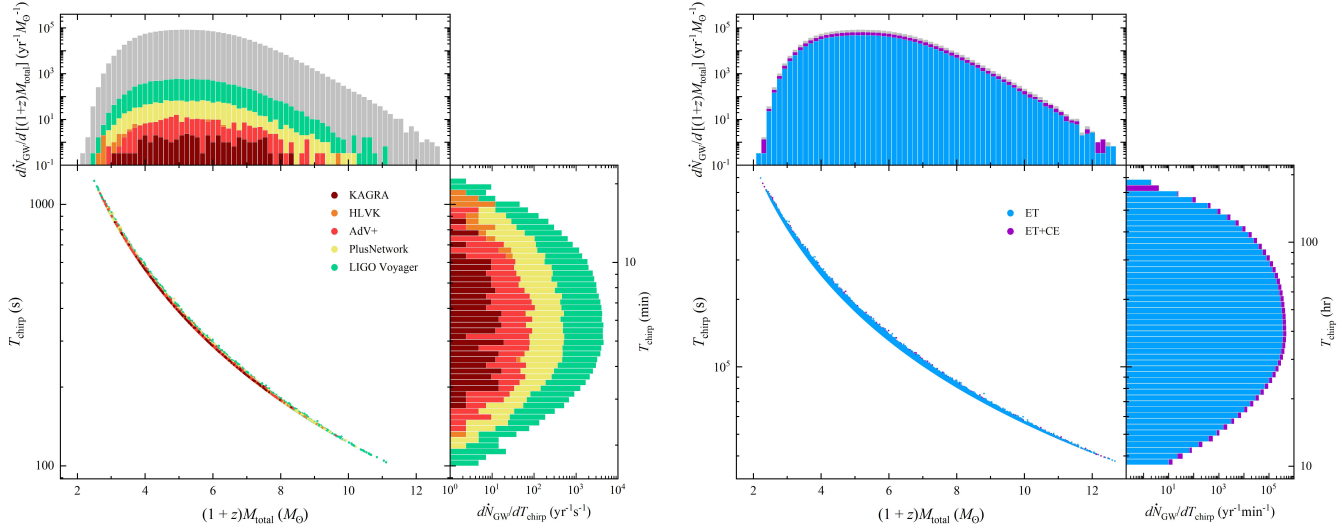


Figure 5. Left panels: the chirp time for the BNS GW signals in 2nd/2.5th generation GW detectors and LIGO Voyager. Right panels: the chirp time for the BNS GW signals in ET and ET&CE. The gray histograms represent the distributions of the geocentric frame total mass for overall BNS merger events in the universe per year.

limit for various γ -ray detectors. In our calculations, we simply set $F_{\gamma, \text{limit}} \sim 10^{-7} \text{ erg s}^{-1}$ in 50 – 300 keV which is the effective sensitivity limit of GECAM (Zhang et al. 2018b).

By reference to the follow-up search of GW170817/GRB170817A/AT2017gfo, the detection of the associated kilonova was initially made in an i -band filter by 1-m telescopes and subsequently confirmed by larger telescopes (Coulter et al. 2017). Similar to this case, we assume that an optimal strategy to search for associated EM signals is taken by using only one filter to make follow-up observations after GW triggers. By assuming that the survey telescopes would not miss the lightcurve peak of the kilonova in each band, the judgement condition for the detection of the associated kilonova and afterglow is $F_{\nu, \text{KN}}(t_{\text{KN}, \text{p}}) + F_{\nu, \text{AG}}(t_{\text{KN}, \text{p}}) > F_{\nu, \text{limit}}$, where $F_{\nu, \text{limit}} = 3631 \text{ Jy} \times 10^{-m_{\text{limit}}/2.5}$ is the effective limiting flux in each band.

4.2.2. Results for ToO Observations after GW Triggers

Table 5 shows the simulated detection rates of four samples during the HLVK (O4) era as a function of the search limiting magnitude in three bands, which are typically used by present and future survey telescopes, i.e., the gri bands. For the same search depth of each filter, it is clear that there is no significant difference between searching in different bands. Since the detection rates of four samples are essentially not influenced by the search filter, we only show the r -band detection rates for four GW detection eras in Figure 6 and list their precise values in Table 6. The r -band limiting magnitude of ZTF,

Mephisto, WFST, LSST, and SiTian, with the 300 s exposure time are also labeled in Figure 6.

In the upcoming HLVK (O4) era, it is clear that the critical magnitude for the detection of EM emissions from all BNS GW events are $m_{\text{limit}} \sim 21.5 \text{ mag}$. Because the detection rates of GW-triggered ToO observations are calculated based on the brightness of total emissions at the peak time of the kilonovae, in order to cover all BNS GW events for searching for their EM signals, a deeper search limiting magnitude of $m_{\text{limit}} \gtrsim 22\text{--}23 \text{ mag}$ is suggested in view of the rapid evolution of the kilonova and afterglow. Thus, with a limiting magnitude of 300 s exposure time, ZTF/SiTian will be capable of finding EM emissions from $\gtrsim 50\%$ of BNS GW events, while other survey projects can cover all events. The amount of observable kilonova in O4 would be handful. One can achieve a maximum detection rate of $\dot{N}_{\text{EM}} \sim 16 \text{ yr}^{-1}$ for the multi-messenger observations of GW and clear kilonova signals. Among these events, a rate of $\dot{N}_{\text{EM}} \sim 4 \text{ yr}^{-1}$, including $\sim 1 \text{ yr}^{-1}$ Platinum sample events and $\sim 3 \text{ yr}^{-1}$ Gold sample events, can have simultaneously observed sGRBs emissions. The other BNS GW events would be afterglow-dominated with a maximum detection rate of $\sim 11 \text{ yr}^{-1}$. The survey projects with a limiting magnitude of $m_{\text{limit}} \lesssim 18 \text{ mag}$ may be hard to search for kilonova signals. However, they can find bright on-axis jet afterglows by following up the detections of sGRBs or orphan afterglows with a much higher probability than detecting kilonovae.

For the future GW eras of PlusNetwork, LIGO Voyager, and ET&CE, the critical magnitudes for the detection of EM emissions from all BNS GW events would be $\sim 23.5 \text{ mag}$, $\sim 25 \text{ mag}$, and $\gtrsim 26 \text{ mag}$, respec-

Table 5. EM Detection Rates in the HLVK Era

Sample	sGRB	$F_{\nu,\text{KN}}(t_{\text{KN,p}}) > 5F_{\nu,\text{AG}}(t_{\text{KN,p}})$	Filter	$m_{\text{limit}} = 18 \text{ mag}$	20 mag	22 mag	24 mag	26 mag
Platinum	\checkmark ($\theta_v > 3\theta_c$)	\checkmark	g	0	0.3	1.5	1.6	1.6
			r	0	0.6	1.6	1.6	1.6
			i	0	0.4	1.6	1.6	1.6
Gold	\checkmark ($\theta_v < 3\theta_c$)	\checkmark	g	0	0.1	2.3	2.4	2.4
			r	0	0.4	2.7	2.7	2.7
			i	0	0.2	2.4	2.4	2.4
Silver	\times	\checkmark	g	0.05	0.8	02	12	12
			r	0.2	1.6	12	12	12
			i	0.3	1.9	12	12	12
Copper	\checkmark & \times	\times	g	2.8	6.7	11	11	11
			r	3.3	7.3	11	11	11
			i	3.5	7.3	11	11	11

NOTE—The values represent the simulated BNS merger detection rates (in unit of yr^{-1}) in the HLVK era for different samples with different 5σ limiting magnitude in gri band.**Table 6.** r -band EM Detection Rates in Each GW Era

Sample	Era	$m_{r,\text{limit}} = 18 \text{ mag}$	19 mag	20 mag	21 mag	22 mag	23 mag	24 mag	25 mag	26 mag
Platinum	HLVK	0	0.1	0.6	1.3	1.6	1.6	1.6	1.6	1.6
	PlusNetwork	0	0.1	0.6	1.3	3.1	4.4	4.5	4.5	4.5
	Voyager	0	0.1	0.6	1.3	3.1	5.2	6.7	6.8	6.8
	ET&CE	0	0.1	0.6	1.3	3.1	5.4	7.1	7.5	7.5
Gold	HLVK	0	0.1	0.4	1.4	2.7	2.7	2.7	2.7	2.7
	PlusNetwork	0	0.1	0.4	1.4	6.0	17	19	19	19
	Voyager	0	0.1	0.4	1.4	5.9	22	56	91	95
	ET&CE	0	0.1	0.4	1.4	6.1	24	75	210	430
Silver	HLVK	0.2	0.4	1.6	6.5	12	12	12	12	12
	PlusNetwork	0.2	0.4	1.6	6.9	35	98	107	107	107
	Voyager	0.2	0.4	1.6	6.9	35	150	510	1.0×10^3	1.0×10^3
	ET&CE	0.2	0.4	1.6	6.9	35	160	770	3.7×10^3	1.5×10^4
Copper	HLVK	3.3	4.8	7.3	10	11	11	11	11	11
	PlusNetwork	8.2	15	26	43	66	80	81	81	81
	Voyager	16	35	71	140	240	390	570	680	680
	ET&CE	32	94	270	700	1.7×10^3	3.7×10^3	7.5×10^3	1.4×10^4	2.4×10^4

NOTE—The values represent the simulated BNS merger detection rates (in unit of yr^{-1}) in different GW eras for different samples with different r -band 5σ limiting magnitude.

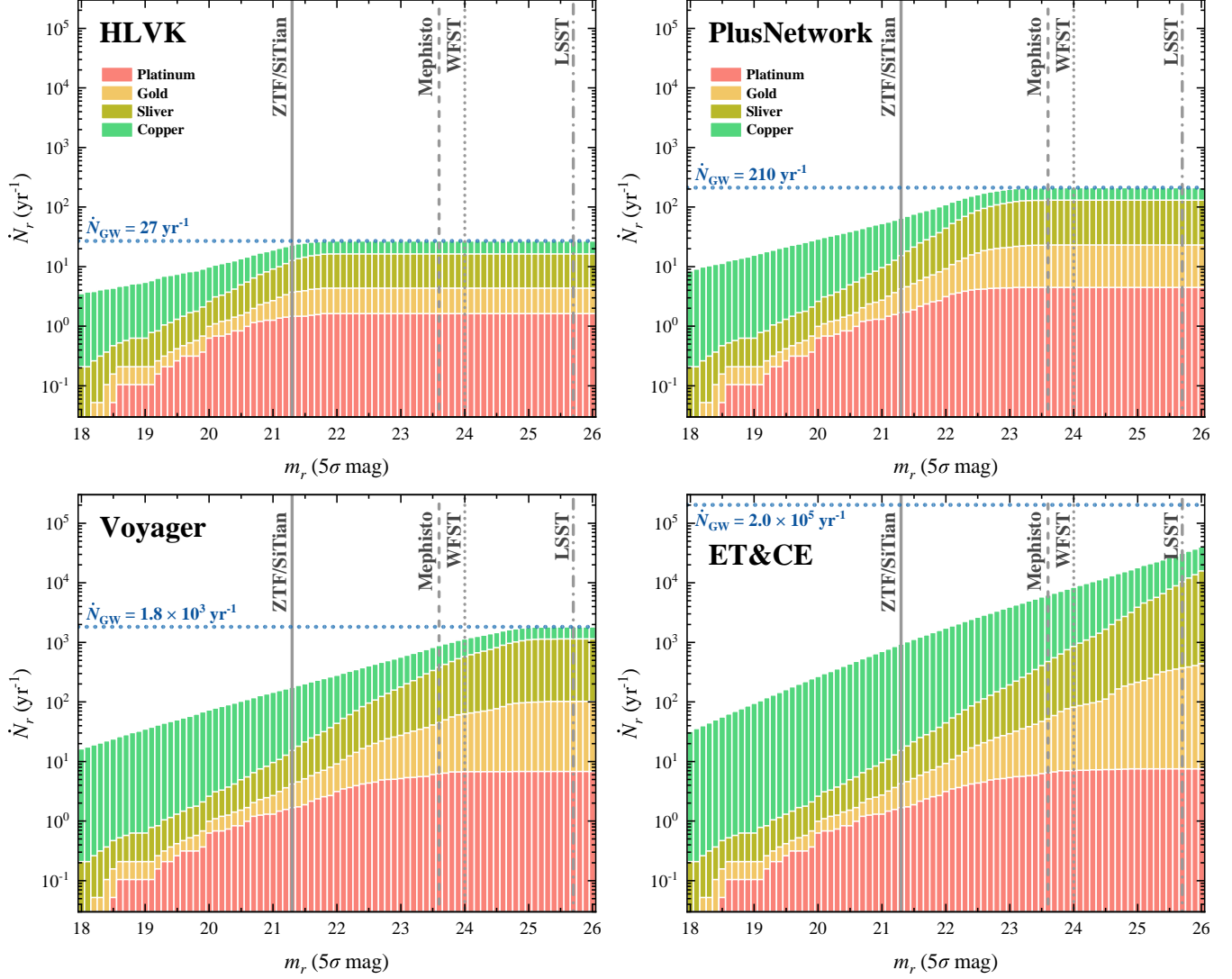


Figure 6. r -band cumulative detection rates for platinum (red histograms), gold (yellow histograms), sliver (dark green histograms), and copper (green histograms) samples as functions of r -band 5σ limiting magnitude during four GW detection eras, i.e., the HLVK, PlusNetwork, LIGO Voyager, and ET&CE eras. The gray solid, dashed, dotted, and dashed-dotted lines respectively represent the r -band 5σ limiting magnitude of ZTF/SiTian, Mephisto, WFST, and LSST, with 300s exposure time. The dashed blue lines show the GW detection rates in each GW era. The bin width of the histograms is set as $\Delta = 0.1$ mag.

tively. Present and foreseeable future survey projects can hardly find all EM signals of BNS GW events detected during the ET&CE era. Comparing with the results of adjacent GW eras, if the limiting magnitude is shallower than the critical magnitudes of earlier GW era, one can see there appears little difference in the number of detectable kilonovae in different GW detection eras. However, one can find much more remote afterglows associated with sGRBs and orphan afterglows (i.e., Copper sample) in the later GW era. As the search limiting magnitude increases, the amount of kilonova-dominated events other than the Platinum sample ones would increase exponentially. There is also an exponential increase with a slower rising slope for the amount of afterglow-dominated BNS GW events of Copper sample. At the critical limiting magnitude of each era, $\sim 60\%$ BNS GW events can observe clear kilonova signals, while afterglow-dominated events would account for the other $\sim 40\%$ BNS GW events. Most of the discovered kilonova-dominated BNS GW events would be placed in the group of Silver sample. The kilonova-dominated events associated with sGRBs, especially for the Platinum sample events like the observations of GW170817/GRB170817A/AT2017gfo, would be scarce.

5. CONCLUSIONS AND DISCUSSION

In this paper, based on our model proposed in the companion paper (Paper I), we have presented the serendipitous search detectability of time-domain surveys for BNS EM signals, the detectability of GWs for different generations of GW detectors, as well as joint-search GW signals and optical EM counterparts.

Serendipitous observations—We have systematically made simulations of optimal search strategy for searching for kilonova and afterglow emissions from BNS mergers by serendipitous observations. For our selected survey projects, which include ZTF/Mephisto/WFST/LSST, we have found that a one-day cadence serendipitous search with an exposure time of ~ 30 s can always achieve near maximum detection rates for kilonovae and afterglows. The optimal detection rate of kilonova-dominated (afterglow-dominated) events are $\sim 0.2/0.5/0.8/20 \text{ yr}^{-1}$ ($\sim 500/300/600/3000 \text{ yr}^{-1}$), respectively, for the survey projects of ZTF/Mephisto/WFST/LSST. As for the survey array of SiTian project, we have shown that when the array fully operates it will discover more kilonova events if a longer exposure time is adopted. The detection rate of kilonova-dominated (afterglow-dominated) events could even reach $\sim 5(6 \times 10^3) \text{ yr}^{-1}$ by SiTian. Our results have shown that afterglows are easier to de-

tect than kilonovae by these survey projects. However, present survey projects have not detected as many afterglows as we have predicted. One reason may be that only part of BNS GW events could generate relativistic jets and power bright afterglows. Genuine weather fluctuations and operational issues of optical telescopes might contribute to the deficit of detection. Actual survey observations can hardly always achieve the prospective detection depth and cadence, which could be another cause of the lack of enough afterglow observations. Furthermore, the relatively longer cadence interval for traditional survey projects have been designed to discover ordinary supernovae or tidal disruption events. These cadence intervals are significantly larger than the timescales during which the brightness of afterglow is above the limiting magnitude (as shown in Table 1), so afterglow events could be easily missed. Recently, thanks to the improved cadence, ZTF has discovered seven independent optically-discovered GRB afterglows without any detection of an associated kilonova (Andreoni et al. 2021b). Among these detected afterglows, at least one event was inferred to be associated with a sGRB. This ZTF observation may support our afterglow simulations, but also show a possible low efficiency of detecting afterglows, especially the off-axis orphan afterglows. Andreoni et al. (2021a,b) intended to select kilonova and afterglow candidates from survey database by considering recorded sources having rising rates faster than 1 mag day^{-1} and fading rates faster than 0.3 mag day^{-1} . However, such selection criteria would miss most orphan afterglows. Since most afterglows discovered via serendipitous observations should be off-axis orphan afterglows without GW triggers, we predicted that there could be orphan afterglows recorded in the survey database which have not been mined. Using color evolution patterns introduced in Paper I, one may be able to discover them from the archival data. Conversely, the low efficiency of afterglow observations also indicate the difficulty for searching for kilonova signals by serendipitous observations.

GW detections—We have carried out detailed calculations of the detection capabilities of the 2nd, 2.5th, and 3rd generation detector networks in the near future for BNS GW signals. We show that the GW detection rates of the worst and best cases for the 2nd generation GW detector network are $\sim 6 \text{ yr}^{-1}$ and $\sim 27 \text{ yr}^{-1}$, respectively. The values of the worst and best detection rates for the 2.5th generation GW detector network would increase to $\sim 34 \text{ yr}^{-1}$ and $\sim 210 \text{ yr}^{-1}$, respectively. For the 3rd generation detector network, LIGO Voyager will be able to detect $\sim 1.8 \times 10^3$ BNS merger events per year. A single ET and the ET&CE network are expected to

detect all BNS merger events in the entire universe, with detection rates $\sim 1.5 \times 10^4 \text{ yr}^{-1}$ and $\sim 2.0 \times 10^4 \text{ yr}^{-1}$, respectively. As the sensitivity of GW detectors increases, BNS events at high redshifts gradually dominate the detected events. For ET and ET&CE, the detection rate is mainly dominated by BNS mergers at $z \sim 1$. We also show the chirp time of the detector networks of different generations. For the 2nd and 2.5th generation detectors and LIGO Voyager, the median chirp time is ~ 6 min. Since the minimum frequency reduces from 10 Hz to 1 Hz for ET and ET&CE, the chirp time would reach the order of days or even a week with a median value close to ~ 2 day, which can provide enough preparation times for EM observations. The detailed GW detection rates, median and maximum detectable distances, chirp time, and total mass in the geocentric frame of detectable GW signals can be consulted from Table 4.

GW-triggered ToO observations—In the upcoming 2nd generation GW detector networks, we have shown that follow-up observations with a limiting magnitude of $m_{\text{limit}} \gtrsim 22 - 23$ mag can discover all EM signals from BNS GW events. Among these detected GW events, $\sim 60\%$ of the events ($\sim 16 \text{ yr}^{-1}$) can display clear kilonova signals, while afterglow-dominated events would account for the other $\sim 40\%$ of the events ($\sim 11 \text{ yr}^{-1}$). In the 2.5th and 3rd(Voyager) generation era, the critical magnitudes for the detection of EM emissions from all BNS GW events would be ~ 23.5 mag and ~ 25 mag, respectively. Present and foreseeable future survey projects can hardly find all EM signals of BNS GW events detected during the ET&CE era. By assuming a single-Gaussian structured jet model (e.g., Zhang & Mészáros 2002), we have shown that GW170817-like events, which can be simultaneously observed as an off-axis sGRB and a clear kilonova, may be scarce. In order to explain the sGRB signal of GW170817/GRB170817A, a two-Gaussian structured jet model may be required (Tan & Yu 2020). Future multi-messenger detection rates of sGRBs, kilonovae and afterglows can be used for constraining the jet structure.

In this paper, we adopt an AT2017gfo-like model as our standard kilonova model to calculate the kilonova detectability of serendipitous and GW-triggered ToO observations. However, many theoretical works in the literature (e.g., Kasen et al. 2013, 2017; Kawaguchi et al. 2020, 2021; Darbha & Kasen 2020; Korobkin et al. 2021; Wollaeger et al. 2021) show that BNS kilonova should be diverse which may depend on the mass ratio of binary and the nature of the merger remnant. The possible energy injection from the merger remnant, e.g., due to spindown of a post-merger magnetar (Yu et al. 2013, 2018; Metzger & Piro 2014; Ai et al. 2018; Li et al. 2018; Ren et al. 2019)³ or fall-back accretion onto the post-merger BH (Rosswog 2007; Ma et al. 2018) could significantly increase the brightness of the kilonova. The diversity of kilonova and potential energy injection may affect on the final detection rate of kilonova, which will be studied in future work.

Software: POSSIS (Bulla 2019; Coughlin et al. 2020b); Matlab, <https://www.mathworks.com>; Python, <https://www.python.org>; LALSuite, (LIGO Scientific Collaboration 2018);

ACKNOWLEDGMENTS

We thank Xue-Feng Wu and Jiming Yu for valuable comments. The work of J.P.Z is partially supported by the National Science Foundation of China under Grant No. 11721303 and the National Basic Research Program of China under grant No. 2014CB845800. Y.P.Y is supported by National Natural Science Foundation of China grant No. 12003028. Z.J.C is supported by the National Natural Science Foundation of China (No. 11690023). H.G. is supported by the National Natural Science Foundation of China under Grant No. 11690024, 12021003, 11633001. Y.W.Y is supported by the National Natural Science Foundation of China under Grant No. 11822302, 11833003.

APPENDIX

A. AMPLITUDE SPECTRAL DENSITY

The ASD sensitivity curves of GW detectors used in our calculations are presented in Figure 7. For O3, we adopt the GW190814's sensitivity curves⁴ as the O3 sensitivity. The detector sensitivities during HLVK, PlusNework and

³ The dissipation of wind from remnant magnetar (Zhang 2013) or interaction between the relativistic magnetar-driven ejecta and the circumstellar medium (Gao et al. 2013a; Liu et al. 2020) may also produce additional optical emission.

⁴ <https://dcc.ligo.org/P2000183/public>

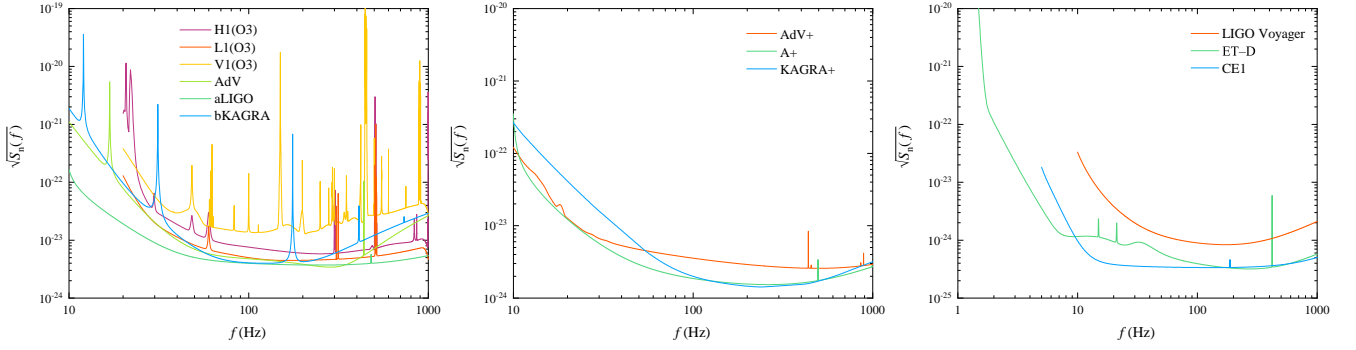


Figure 7. Left panel: the design sensitivity curves of 2nd generation GW detectors and O3 sensitivity curves. Middle panel: the design sensitivity curves of 2.5th generation GW detectors. Right panel: the design sensitivity curves of 3rd generation GW detectors.

LIGO Voyager era are adopted from the public data⁵⁶⁷. The sensitivity curves of ET and CE used in this paper come from the official websites⁸⁹.

REFERENCES

- Abbott, B. P., Abbott, R., Abbott, T. D., et al. 2017a, *PhRvL*, 119, 161101, doi: [10.1103/PhysRevLett.119.161101](https://doi.org/10.1103/PhysRevLett.119.161101)
- . 2017b, *ApJL*, 848, L13, doi: [10.3847/2041-8213/aa920c](https://doi.org/10.3847/2041-8213/aa920c)
- . 2017c, *ApJL*, 848, L12, doi: [10.3847/2041-8213/aa91c9](https://doi.org/10.3847/2041-8213/aa91c9)
- . 2019, *Physical Review X*, 9, 011001, doi: [10.1103/PhysRevX.9.011001](https://doi.org/10.1103/PhysRevX.9.011001)
- . 2020, *Living Reviews in Relativity*, 23, 3, doi: [10.1007/s41114-020-00026-9](https://doi.org/10.1007/s41114-020-00026-9)
- Abbott, R., Abbott, T. D., Abraham, S., et al. 2021a, *ApJL*, 915, L5, doi: [10.3847/2041-8213/ac082e](https://doi.org/10.3847/2041-8213/ac082e)
- . 2021b, *ApJL*, 913, L7, doi: [10.3847/2041-8213/abe949](https://doi.org/10.3847/2041-8213/abe949)
- . 2021c, *Physical Review X*, 11, 021053, doi: [10.1103/PhysRevX.11.021053](https://doi.org/10.1103/PhysRevX.11.021053)
- Acernese, F., Agathos, M., Agatsuma, K., et al. 2015, *Classical and Quantum Gravity*, 32, 024001, doi: [10.1088/0264-9381/32/2/024001](https://doi.org/10.1088/0264-9381/32/2/024001)
- Adhikari, R. X., Arai, K., Brooks, A. F., et al. 2020, *Classical and Quantum Gravity*, 37, 165003, doi: [10.1088/1361-6382/ab9143](https://doi.org/10.1088/1361-6382/ab9143)
- Ai, S., Gao, H., Dai, Z.-G., et al. 2018, *ApJ*, 860, 57, doi: [10.3847/1538-4357/aac2b7](https://doi.org/10.3847/1538-4357/aac2b7)
- Alexander, K. D., Berger, E., Fong, W., et al. 2017, *ApJL*, 848, L21, doi: [10.3847/2041-8213/aa905d](https://doi.org/10.3847/2041-8213/aa905d)
- Allen, B., Anderson, W. G., Brady, P. R., Brown, D. A., & Creighton, J. D. E. 2012, *PhRvD*, 85, 122006, doi: [10.1103/PhysRevD.85.122006](https://doi.org/10.1103/PhysRevD.85.122006)
- Almualla, M., Anand, S., Coughlin, M. W., et al. 2021, *MNRAS*, 504, 2822, doi: [10.1093/mnras/stab1090](https://doi.org/10.1093/mnras/stab1090)
- Andreoni, I., Ackley, K., Cooke, J., et al. 2017, *PASA*, 34, e069, doi: [10.1017/pasa.2017.65](https://doi.org/10.1017/pasa.2017.65)
- Andreoni, I., Coughlin, M. W., Almualla, M., et al. 2021a, *arXiv e-prints*, arXiv:2106.06820, <https://arxiv.org/abs/2106.06820>
- Andreoni, I., Coughlin, M. W., Kool, E. C., et al. 2021b, *ApJ*, 918, 63, doi: [10.3847/1538-4357/ac0bc7](https://doi.org/10.3847/1538-4357/ac0bc7)
- Arcavi, I., Hosseinzadeh, G., Howell, D. A., et al. 2017, *Nature*, 551, 64, doi: [10.1038/nature24291](https://doi.org/10.1038/nature24291)
- Ascenzi, S., Coughlin, M. W., Dietrich, T., et al. 2019, *MNRAS*, 486, 672, doi: [10.1093/mnras/stz891](https://doi.org/10.1093/mnras/stz891)
- Aso, Y., Michimura, Y., Somiya, K., et al. 2013, *PhRvD*, 88, 043007, doi: [10.1103/PhysRevD.88.043007](https://doi.org/10.1103/PhysRevD.88.043007)
- Bellm, E. C., Kulkarni, S. R., Graham, M. J., et al. 2019, *PASP*, 131, 018002, doi: [10.1088/1538-3873/aacbe](https://doi.org/10.1088/1538-3873/aacbe)
- Berger, E., Fong, W., & Chornock, R. 2013, *ApJL*, 774, L23, doi: [10.1088/2041-8205/774/2/L23](https://doi.org/10.1088/2041-8205/774/2/L23)
- Broekgaarden, F. S., Berger, E., Neijssel, C. J., et al. 2021, *arXiv e-prints*, arXiv:2103.02608, <https://arxiv.org/abs/2103.02608>
- Bulla, M. 2019, *MNRAS*, 489, 5037, doi: [10.1093/mnras/stz2495](https://doi.org/10.1093/mnras/stz2495)
- ⁵ <https://dcc.ligo.org/LIGO-P1200087-v42/public>
- ⁶ <https://gwdoc.icrr.u-tokyo.ac.jp/cgi-bin/DocDB/ShowDocument?docid=9537>
- ⁷ <https://dcc.ligo.org/LIGO-T1500293/public>
- ⁸ <http://www.et-gw.eu/index.php/etsensitivities>
- ⁹ <https://dcc.cosmicexplorer.org/cgi-bin/DocDB/ShowDocument?docid=T2000017>

- Chan, M. L., Messenger, C., Heng, I. S., & Hendry, M. 2018, *PhRvD*, 97, 123014, doi: [10.1103/PhysRevD.97.123014](https://doi.org/10.1103/PhysRevD.97.123014)
- Chase, E. A., O'Connor, B., Fryer, C. L., et al. 2021, arXiv e-prints, arXiv:2105.12268, <https://arxiv.org/abs/2105.12268>
- Cheng, K. S., & Wang, J.-M. 1999, *ApJ*, 521, 502, doi: [10.1086/307572](https://doi.org/10.1086/307572)
- Chornock, R., Berger, E., Kasen, D., et al. 2017, *ApJL*, 848, L19, doi: [10.3847/2041-8213/aa905c](https://doi.org/10.3847/2041-8213/aa905c)
- Coughlin, M., Dietrich, T., Kawaguchi, K., et al. 2017, *ApJ*, 849, 12, doi: [10.3847/1538-4357/aa9114](https://doi.org/10.3847/1538-4357/aa9114)
- Coughlin, M. W., Dietrich, T., Antier, S., et al. 2020a, *MNRAS*, 497, 1181, doi: [10.1093/mnras/staa1925](https://doi.org/10.1093/mnras/staa1925)
- Coughlin, M. W., Antier, S., Dietrich, T., et al. 2020b, *Nature Communications*, 11, 4129, doi: [10.1038/s41467-020-17998-5](https://doi.org/10.1038/s41467-020-17998-5)
- Coulter, D. A., Foley, R. J., Kilpatrick, C. D., et al. 2017, *Science*, 358, 1556, doi: [10.1126/science.aap9811](https://doi.org/10.1126/science.aap9811)
- Covino, S., Wiersema, K., Fan, Y. Z., et al. 2017, *Nature Astronomy*, 1, 791, doi: [10.1038/s41550-017-0285-z](https://doi.org/10.1038/s41550-017-0285-z)
- Cowperthwaite, P. S., Villar, V. A., Scolnic, D. M., & Berger, E. 2019, *ApJ*, 874, 88, doi: [10.3847/1538-4357/ab07b6](https://doi.org/10.3847/1538-4357/ab07b6)
- Cowperthwaite, P. S., Berger, E., Villar, V. A., et al. 2017, *ApJL*, 848, L17, doi: [10.3847/2041-8213/aa8fc7](https://doi.org/10.3847/2041-8213/aa8fc7)
- Darbha, S., & Kasen, D. 2020, *ApJ*, 897, 150, doi: [10.3847/1538-4357/ab9a34](https://doi.org/10.3847/1538-4357/ab9a34)
- D'Avanzo, P., Campana, S., Salafia, O. S., et al. 2018, *A&A*, 613, L1, doi: [10.1051/0004-6361/201832664](https://doi.org/10.1051/0004-6361/201832664)
- Díaz, M. C., Macri, L. M., Garcia Lambas, D., et al. 2017, *ApJL*, 848, L29, doi: [10.3847/2041-8213/aa9060](https://doi.org/10.3847/2041-8213/aa9060)
- Dietrich, T., Samajdar, A., Khan, S., et al. 2019, *PhRvD*, 100, 044003, doi: [10.1103/PhysRevD.100.044003](https://doi.org/10.1103/PhysRevD.100.044003)
- Dobie, D., Kaplan, D. L., Murphy, T., et al. 2018, *ApJL*, 858, L15, doi: [10.3847/2041-8213/aac105](https://doi.org/10.3847/2041-8213/aac105)
- Drout, M. R., Piro, A. L., Shappee, B. J., et al. 2017, *Science*, 358, 1570, doi: [10.1126/science.aag0049](https://doi.org/10.1126/science.aag0049)
- Drozda, P., Belczynski, K., O'Shaughnessy, R., Bulik, T., & Fryer, C. L. 2020, arXiv e-prints, arXiv:2009.06655, <https://arxiv.org/abs/2009.06655>
- Eichler, D., Livio, M., Piran, T., & Schramm, D. N. 1989, *Nature*, 340, 126, doi: [10.1038/340126a0](https://doi.org/10.1038/340126a0)
- Evans, P. A., Cenko, S. B., Kennea, J. A., et al. 2017, *Science*, 358, 1565, doi: [10.1126/science.aap9580](https://doi.org/10.1126/science.aap9580)
- Fan, Y.-Z., Yu, Y.-W., Xu, D., et al. 2013, *ApJL*, 779, L25, doi: [10.1088/2041-8205/779/2/L25](https://doi.org/10.1088/2041-8205/779/2/L25)
- Fong, W., Laskar, T., Rastinejad, J., et al. 2021, *ApJ*, 906, 127, doi: [10.3847/1538-4357/abc74a](https://doi.org/10.3847/1538-4357/abc74a)
- Frostig, D., Biscoveanu, S., Mo, G., et al. 2021, arXiv e-prints, arXiv:2110.01622, <https://arxiv.org/abs/2110.01622>
- Gao, H., Ding, X., Wu, X.-F., Dai, Z.-G., & Zhang, B. 2015, *ApJ*, 807, 163, doi: [10.1088/0004-637X/807/2/163](https://doi.org/10.1088/0004-637X/807/2/163)
- Gao, H., Ding, X., Wu, X.-F., Zhang, B., & Dai, Z.-G. 2013a, *ApJ*, 771, 86, doi: [10.1088/0004-637X/771/2/86](https://doi.org/10.1088/0004-637X/771/2/86)
- Gao, H., Lei, W.-H., Zou, Y.-C., Wu, X.-F., & Zhang, B. 2013b, *NewAR*, 57, 141, doi: [10.1016/j.newar.2013.10.001](https://doi.org/10.1016/j.newar.2013.10.001)
- Gao, H., Zhang, B., & Lü, H.-J. 2016, *PhRvD*, 93, 044065, doi: [10.1103/PhysRevD.93.044065](https://doi.org/10.1103/PhysRevD.93.044065)
- Gao, H., Zhang, B., Lü, H.-J., & Li, Y. 2017, *ApJ*, 837, 50, doi: [10.3847/1538-4357/aa5be3](https://doi.org/10.3847/1538-4357/aa5be3)
- Ghirlanda, G., Salafia, O. S., Paragi, Z., et al. 2019, *Science*, 363, 968, doi: [10.1126/science.aau8815](https://doi.org/10.1126/science.aau8815)
- Goldstein, A., Veres, P., Burns, E., et al. 2017, *ApJL*, 848, L14, doi: [10.3847/2041-8213/aa8f41](https://doi.org/10.3847/2041-8213/aa8f41)
- Gompertz, B. P., Levan, A. J., Tanvir, N. R., et al. 2018, *ApJ*, 860, 62, doi: [10.3847/1538-4357/aac206](https://doi.org/10.3847/1538-4357/aac206)
- Haggard, D., Nynka, M., Ruan, J. J., et al. 2017, *ApJL*, 848, L25, doi: [10.3847/2041-8213/aa8ede](https://doi.org/10.3847/2041-8213/aa8ede)
- Hallinan, G., Corsi, A., Mooley, K. P., et al. 2017, *Science*, 358, 1579, doi: [10.1126/science.aap9855](https://doi.org/10.1126/science.aap9855)
- Harry, G. M., & LIGO Scientific Collaboration. 2010, *Classical and Quantum Gravity*, 27, 084006, doi: [10.1088/0264-9381/27/8/084006](https://doi.org/10.1088/0264-9381/27/8/084006)
- Hu, L., Wu, X., Andreoni, I., et al. 2017, *Science Bulletin*, 62, 1433, doi: [10.1016/j.scib.2017.10.006](https://doi.org/10.1016/j.scib.2017.10.006)
- Jin, Z.-P., Covino, S., Liao, N.-H., et al. 2020, *Nature Astronomy*, 4, 77, doi: [10.1038/s41550-019-0892-y](https://doi.org/10.1038/s41550-019-0892-y)
- Jin, Z.-P., Li, X., Cano, Z., et al. 2015, *ApJL*, 811, L22, doi: [10.1088/2041-8205/811/2/L22](https://doi.org/10.1088/2041-8205/811/2/L22)
- Jin, Z.-P., Hotokezaka, K., Li, X., et al. 2016, *Nature Communications*, 7, 12898, doi: [10.1038/ncomms12898](https://doi.org/10.1038/ncomms12898)
- Kagra Collaboration, Akutsu, T., Ando, M., et al. 2019, *Nature Astronomy*, 3, 35, doi: [10.1038/s41550-018-0658-y](https://doi.org/10.1038/s41550-018-0658-y)
- Kapadia, S. J., Singh, M. K., Shaikh, M. A., Chatterjee, D., & Ajith, P. 2020, *ApJL*, 898, L39, doi: [10.3847/2041-8213/aba42d](https://doi.org/10.3847/2041-8213/aba42d)
- Kasen, D., Badnell, N. R., & Barnes, J. 2013, *ApJ*, 774, 25, doi: [10.1088/0004-637X/774/1/25](https://doi.org/10.1088/0004-637X/774/1/25)
- Kasen, D., Metzger, B., Barnes, J., Quataert, E., & Ramirez-Ruiz, E. 2017, *Nature*, 551, 80, doi: [10.1038/nature24453](https://doi.org/10.1038/nature24453)
- Kasliwal, M. M., Nakar, E., Singer, L. P., et al. 2017, *Science*, 358, 1559, doi: [10.1126/science.aap9455](https://doi.org/10.1126/science.aap9455)
- Kasliwal, M. M., Anand, S., Ahumada, T., et al. 2020, *ApJ*, 905, 145, doi: [10.3847/1538-4357/abc335](https://doi.org/10.3847/1538-4357/abc335)

- Kawaguchi, K., Fujibayashi, S., Shibata, M., Tanaka, M., & Wanajo, S. 2021, *ApJ*, 913, 100, doi: [10.3847/1538-4357/abf3bc](https://doi.org/10.3847/1538-4357/abf3bc)
- Kawaguchi, K., Shibata, M., & Tanaka, M. 2020, *ApJ*, 889, 171, doi: [10.3847/1538-4357/ab61f6](https://doi.org/10.3847/1538-4357/ab61f6)
- Kilpatrick, C. D., Foley, R. J., Kasen, D., et al. 2017, *Science*, 358, 1583, doi: [10.1126/science.aag0073](https://doi.org/10.1126/science.aag0073)
- Kiziltan, B., Kottas, A., De Yoreo, M., & Thorsett, S. E. 2013, *ApJ*, 778, 66, doi: [10.1088/0004-637X/778/1/66](https://doi.org/10.1088/0004-637X/778/1/66)
- Korobkin, O., Wollaeger, R. T., Fryer, C. L., et al. 2021, *ApJ*, 910, 116, doi: [10.3847/1538-4357/abe1b5](https://doi.org/10.3847/1538-4357/abe1b5)
- Lattimer, J. M. 2012, *Annual Review of Nuclear and Particle Science*, 62, 485, doi: [10.1146/annurev-nucl-102711-095018](https://doi.org/10.1146/annurev-nucl-102711-095018)
- Lazzati, D., Perna, R., Morsony, B. J., et al. 2018, *PhRvL*, 120, 241103, doi: [10.1103/PhysRevLett.120.241103](https://doi.org/10.1103/PhysRevLett.120.241103)
- Lei, L., Li, J., Wu, J., Jiang, S., & Chen, B. 2021, *Astronomical Research & Technology*, 18, L18, doi: [10.14005/j.cnki.issn1672-7673.20200713.001](https://doi.org/10.14005/j.cnki.issn1672-7673.20200713.001)
- Li, L.-X., & Paczyński, B. 1998, *ApJL*, 507, L59, doi: [10.1086/311680](https://doi.org/10.1086/311680)
- Li, S.-Z., Liu, L.-D., Yu, Y.-W., & Zhang, B. 2018, *ApJL*, 861, L12, doi: [10.3847/2041-8213/aace61](https://doi.org/10.3847/2041-8213/aace61)
- LIGO Scientific Collaboration. 2018, *LIGO Algorithm Library - LALSuite*, free software (GPL), doi: [10.7935/GT1W-FZ16](https://doi.org/10.7935/GT1W-FZ16)
- LIGO Scientific Collaboration, Aasi, J., Abbott, B. P., et al. 2015, *Classical and Quantum Gravity*, 32, 074001, doi: [10.1088/0264-9381/32/7/074001](https://doi.org/10.1088/0264-9381/32/7/074001)
- Lipunov, V. M., Gorboskovy, E., Kornilov, V. G., et al. 2017, *ApJL*, 850, L1, doi: [10.3847/2041-8213/aa92c0](https://doi.org/10.3847/2041-8213/aa92c0)
- Liu, J., Soria, R., Wu, X.-F., Wu, H., & Shang, Z. 2021, *An. Acad. Bras. Ciênc. vol.93 supl.1*, 93, 20200628, doi: [10.1590/0001-3765202120200628](https://doi.org/10.1590/0001-3765202120200628)
- Liu, L.-D., Gao, H., & Zhang, B. 2020, *ApJ*, 890, 102, doi: [10.3847/1538-4357/ab6b24](https://doi.org/10.3847/1538-4357/ab6b24)
- LSST Science Collaboration, Abell, P. A., Allison, J., et al. 2009, *arXiv e-prints*, arXiv:0912.0201. <https://arxiv.org/abs/0912.0201>
- Lyman, J. D., Lamb, G. P., Levan, A. J., et al. 2018, *Nature Astronomy*, 2, 751, doi: [10.1038/s41550-018-0511-3](https://doi.org/10.1038/s41550-018-0511-3)
- Ma, S.-B., Lei, W.-H., Gao, H., et al. 2018, *ApJL*, 852, L5, doi: [10.3847/2041-8213/aaa0cd](https://doi.org/10.3847/2041-8213/aaa0cd)
- Ma, S.-B., Xie, W., Liao, B., et al. 2021, *ApJ*, 911, 97, doi: [10.3847/1538-4357/abe71b](https://doi.org/10.3847/1538-4357/abe71b)
- Maggiore, M., Van Den Broeck, C., Bartolo, N., et al. 2020, *JCAP*, 2020, 050, doi: [10.1088/1475-7516/2020/03/050](https://doi.org/10.1088/1475-7516/2020/03/050)
- Mandel, I., & Broekgaarden, F. S. 2021, *arXiv e-prints*, arXiv:2107.14239. <https://arxiv.org/abs/2107.14239>
- Margutti, R., Berger, E., Fong, W., et al. 2017, *ApJL*, 848, L20, doi: [10.3847/2041-8213/aa9057](https://doi.org/10.3847/2041-8213/aa9057)
- Masci, F. J., Laher, R. R., Rusholme, B., et al. 2019, *PASP*, 131, 018003, doi: [10.1088/1538-3873/aae8ac](https://doi.org/10.1088/1538-3873/aae8ac)
- McCully, C., Hiramatsu, D., Howell, D. A., et al. 2017, *ApJL*, 848, L32, doi: [10.3847/2041-8213/aa9111](https://doi.org/10.3847/2041-8213/aa9111)
- McKernan, B., Ford, K. E. S., & O’Shaughnessy, R. 2020, *MNRAS*, 498, 4088, doi: [10.1093/mnras/staa2681](https://doi.org/10.1093/mnras/staa2681)
- Meszaros, P., & Rees, M. J. 1993, *ApJ*, 405, 278, doi: [10.1086/172360](https://doi.org/10.1086/172360)
- Mészáros, P., & Rees, M. J. 1997, *ApJ*, 476, 232, doi: [10.1086/303625](https://doi.org/10.1086/303625)
- Metzger, B. D., & Berger, E. 2012, *ApJ*, 746, 48, doi: [10.1088/0004-637X/746/1/48](https://doi.org/10.1088/0004-637X/746/1/48)
- Metzger, B. D., & Piro, A. L. 2014, *MNRAS*, 439, 3916, doi: [10.1093/mnras/stu247](https://doi.org/10.1093/mnras/stu247)
- Metzger, B. D., Martínez-Pinedo, G., Darbha, S., et al. 2010, *MNRAS*, 406, 2650, doi: [10.1111/j.1365-2966.2010.16864.x](https://doi.org/10.1111/j.1365-2966.2010.16864.x)
- Michimura, Y., Komori, K., Enomoto, Y., et al. 2020, *PhRvD*, 102, 022008, doi: [10.1103/PhysRevD.102.022008](https://doi.org/10.1103/PhysRevD.102.022008)
- Miller, J., Barsotti, L., Vitale, S., et al. 2015, *PhRvD*, 91, 062005, doi: [10.1103/PhysRevD.91.062005](https://doi.org/10.1103/PhysRevD.91.062005)
- Mohite, S. R., Rajkumar, P., Anand, S., et al. 2021, *arXiv e-prints*, arXiv:2107.07129. <https://arxiv.org/abs/2107.07129>
- Narayan, R., Paczynski, B., & Piran, T. 1992, *ApJL*, 395, L83, doi: [10.1086/186493](https://doi.org/10.1086/186493)
- Nicholl, M., Berger, E., Kasen, D., et al. 2017, *ApJL*, 848, L18, doi: [10.3847/2041-8213/aa9029](https://doi.org/10.3847/2041-8213/aa9029)
- Nitz, A. H., Schäfer, M., & Dal Canton, T. 2020, *ApJL*, 902, L29, doi: [10.3847/2041-8213/abbc10](https://doi.org/10.3847/2041-8213/abbc10)
- Paczynski, B. 1986, *ApJL*, 308, L43, doi: [10.1086/184740](https://doi.org/10.1086/184740)
- . 1991, *AcA*, 41, 257
- Paczynski, B., & Rhoads, J. E. 1993, *ApJL*, 418, L5, doi: [10.1086/187102](https://doi.org/10.1086/187102)
- Perna, R., Lazzati, D., & Cantiello, M. 2021, *ApJL*, 906, L7, doi: [10.3847/2041-8213/abd319](https://doi.org/10.3847/2041-8213/abd319)
- Pian, E., D’Avanzo, P., Benetti, S., et al. 2017, *Nature*, 551, 67, doi: [10.1038/nature24298](https://doi.org/10.1038/nature24298)
- Piro, L., Troja, E., Zhang, B., et al. 2019, *MNRAS*, 483, 1912, doi: [10.1093/mnras/sty3047](https://doi.org/10.1093/mnras/sty3047)
- Planck Collaboration, Ade, P. A. R., Aghanim, N., et al. 2016, *A&A*, 594, A13, doi: [10.1051/0004-6361/201525830](https://doi.org/10.1051/0004-6361/201525830)
- Punturo, M., Abernathy, M., Acernese, F., et al. 2010a, *Classical and Quantum Gravity*, 27, 194002, doi: [10.1088/0264-9381/27/19/194002](https://doi.org/10.1088/0264-9381/27/19/194002)
- . 2010b, *Classical and Quantum Gravity*, 27, 084007, doi: [10.1088/0264-9381/27/8/084007](https://doi.org/10.1088/0264-9381/27/8/084007)

- Rees, M. J., & Meszaros, P. 1992, *MNRAS*, 258, 41, doi: [10.1093/mnras/258.1.41P](https://doi.org/10.1093/mnras/258.1.41P)
- Reitze, D., Adhikari, R. X., Ballmer, S., et al. 2019, in *Bulletin of the American Astronomical Society*, Vol. 51, 35. <https://arxiv.org/abs/1907.04833>
- Ren, J., Lin, D.-B., Zhang, L.-L., et al. 2019, *ApJ*, 885, 60, doi: [10.3847/1538-4357/ab4188](https://doi.org/10.3847/1538-4357/ab4188)
- Rossi, A., Stratta, G., Maiorano, E., et al. 2020, *MNRAS*, 493, 3379, doi: [10.1093/mnras/staa479](https://doi.org/10.1093/mnras/staa479)
- Rosswog, S. 2007, *MNRAS*, 376, L48, doi: [10.1111/j.1745-3933.2007.00284.x](https://doi.org/10.1111/j.1745-3933.2007.00284.x)
- Rosswog, S., Feindt, U., Korobkin, O., et al. 2017, *Classical and Quantum Gravity*, 34, 104001, doi: [10.1088/1361-6382/aa68a9](https://doi.org/10.1088/1361-6382/aa68a9)
- Sachdev, S., Magee, R., Hanna, C., et al. 2020, *ApJL*, 905, L25, doi: [10.3847/2041-8213/abc753](https://doi.org/10.3847/2041-8213/abc753)
- Sagués Carracedo, A., Bulla, M., Feindt, U., & Goobar, A. 2021, *MNRAS*, 504, 1294, doi: [10.1093/mnras/stab872](https://doi.org/10.1093/mnras/stab872)
- Sari, R., Piran, T., & Narayan, R. 1998, *ApJL*, 497, L17, doi: [10.1086/311269](https://doi.org/10.1086/311269)
- Savchenko, V., Ferrigno, C., Kuulkers, E., et al. 2017, *ApJL*, 848, L15, doi: [10.3847/2041-8213/aa8f94](https://doi.org/10.3847/2041-8213/aa8f94)
- Scolnic, D., Kessler, R., Brout, D., et al. 2018, *ApJL*, 852, L3, doi: [10.3847/2041-8213/aa9d82](https://doi.org/10.3847/2041-8213/aa9d82)
- Setzer, C. N., Biswas, R., Peiris, H. V., et al. 2019, *MNRAS*, 485, 4260, doi: [10.1093/mnras/stz506](https://doi.org/10.1093/mnras/stz506)
- Shappee, B. J., Simon, J. D., Drout, M. R., et al. 2017, *Science*, 358, 1574, doi: [10.1126/science.aaq0186](https://doi.org/10.1126/science.aaq0186)
- Shi, D.-D., Zheng, X.-Z., Zhao, H.-B., et al. 2018, *ACTA ASTRONOMICA SINICA*, 59, 1, doi: [10.15940/j.cnki.0001-5245.2018.03.001](https://doi.org/10.15940/j.cnki.0001-5245.2018.03.001)
- Singh, M. K., Kapadia, S. J., Shaikh, M. A., Chatterjee, D., & Ajith, P. 2021, *MNRAS*, 502, 1612, doi: [10.1093/mnras/stab125](https://doi.org/10.1093/mnras/stab125)
- Smartt, S. J., Chen, T. W., Jerkstrand, A., et al. 2017, *Nature*, 551, 75, doi: [10.1038/nature24303](https://doi.org/10.1038/nature24303)
- Soares-Santos, M., Holz, D. E., Annis, J., et al. 2017, *ApJL*, 848, L16, doi: [10.3847/2041-8213/aa9059](https://doi.org/10.3847/2041-8213/aa9059)
- Song, H.-R., Ai, S.-K., Wang, M.-H., et al. 2019, *ApJL*, 881, L40, doi: [10.3847/2041-8213/ab3921](https://doi.org/10.3847/2041-8213/ab3921)
- Sun, H., Zhang, B., & Li, Z. 2015, *ApJ*, 812, 33, doi: [10.1088/0004-637X/812/1/33](https://doi.org/10.1088/0004-637X/812/1/33)
- Tan, W.-W., & Yu, Y.-W. 2020, *ApJ*, 902, 83, doi: [10.3847/1538-4357/abb404](https://doi.org/10.3847/1538-4357/abb404)
- Tanvir, N. R., Levan, A. J., Fruchter, A. S., et al. 2013, *Nature*, 500, 547, doi: [10.1038/nature12505](https://doi.org/10.1038/nature12505)
- Tanvir, N. R., Levan, A. J., González-Fernández, C., et al. 2017, *ApJL*, 848, L27, doi: [10.3847/2041-8213/aa90b6](https://doi.org/10.3847/2041-8213/aa90b6)
- Troja, E., Piro, L., van Eerten, H., et al. 2017, *Nature*, 551, 71, doi: [10.1038/nature24290](https://doi.org/10.1038/nature24290)
- Troja, E., Piro, L., Ryan, G., et al. 2018, *MNRAS*, 478, L18, doi: [10.1093/mnrasl/sly061](https://doi.org/10.1093/mnrasl/sly061)
- Troja, E., van Eerten, H., Zhang, B., et al. 2020, *MNRAS*, 498, 5643, doi: [10.1093/mnras/staa2626](https://doi.org/10.1093/mnras/staa2626)
- Typel, S., Röpke, G., Klähn, T., Blaschke, D., & Wolter, H. H. 2010, *PhRvC*, 81, 015803, doi: [10.1103/PhysRevC.81.015803](https://doi.org/10.1103/PhysRevC.81.015803)
- Utsumi, Y., Tanaka, M., Tominaga, N., et al. 2017, *PASJ*, 69, 101, doi: [10.1093/pasj/psx118](https://doi.org/10.1093/pasj/psx118)
- Valenti, S., Sand, D. J., Yang, S., et al. 2017, *ApJL*, 848, L24, doi: [10.3847/2041-8213/aa8edf](https://doi.org/10.3847/2041-8213/aa8edf)
- Villar, V. A., Guillochon, J., Berger, E., et al. 2017, *ApJL*, 851, L21, doi: [10.3847/2041-8213/aa9c84](https://doi.org/10.3847/2041-8213/aa9c84)
- Virgili, F. J., Zhang, B., O'Brien, P., & Troja, E. 2011, *ApJ*, 727, 109, doi: [10.1088/0004-637X/727/2/109](https://doi.org/10.1088/0004-637X/727/2/109)
- Vitale, S., & Evans, M. 2017, *PhRvD*, 95, 064052, doi: [10.1103/PhysRevD.95.064052](https://doi.org/10.1103/PhysRevD.95.064052)
- Vitale, S., & Whittle, C. 2018, *PhRvD*, 98, 024029, doi: [10.1103/PhysRevD.98.024029](https://doi.org/10.1103/PhysRevD.98.024029)
- Wanderman, D., & Piran, T. 2015, *MNRAS*, 448, 3026, doi: [10.1093/mnras/stv123](https://doi.org/10.1093/mnras/stv123)
- Wang, X. L., Zheng, X., Xiao, S., et al. 2021, arXiv e-prints, arXiv:2107.10452. <https://arxiv.org/abs/2107.10452>
- Wen, J., Long, X., Zheng, X., et al. 2019, *Experimental Astronomy*, 48, 77, doi: [10.1007/s10686-019-09636-w](https://doi.org/10.1007/s10686-019-09636-w)
- Wollaeger, R. T., Fryer, C. L., Chase, E. A., et al. 2021, *ApJ*, 918, 10, doi: [10.3847/1538-4357/ac0d03](https://doi.org/10.3847/1538-4357/ac0d03)
- Wu, G.-L., Yu, Y.-W., & Zhu, J.-P. 2021, arXiv e-prints, arXiv:2108.01349. <https://arxiv.org/abs/2108.01349>
- Xie, X., Zrake, J., & MacFadyen, A. 2018, *ApJ*, 863, 58, doi: [10.3847/1538-4357/aac9c](https://doi.org/10.3847/1538-4357/aac9c)
- Yang, B., Jin, Z.-P., Li, X., et al. 2015, *Nature Communications*, 6, 7323, doi: [10.1038/ncomms8323](https://doi.org/10.1038/ncomms8323)
- Yu, J., Song, H., Ai, S., et al. 2021, *ApJ*, 916, 54, doi: [10.3847/1538-4357/ac0628](https://doi.org/10.3847/1538-4357/ac0628)
- Yu, Y.-W., Liu, L.-D., & Dai, Z.-G. 2018, *ApJ*, 861, 114, doi: [10.3847/1538-4357/aac6e5](https://doi.org/10.3847/1538-4357/aac6e5)
- Yu, Y.-W., Zhang, B., & Gao, H. 2013, *ApJL*, 776, L40, doi: [10.1088/2041-8205/776/2/L40](https://doi.org/10.1088/2041-8205/776/2/L40)
- Yuan, Y., Lü, H.-J., Yuan, H.-Y., et al. 2021, *ApJ*, 912, 14, doi: [10.3847/1538-4357/abedb1](https://doi.org/10.3847/1538-4357/abedb1)
- Zappa, F., Bernuzzi, S., Pannarale, F., Mapelli, M., & Giacobbo, N. 2019, *PhRvL*, 123, 041102, doi: [10.1103/PhysRevLett.123.041102](https://doi.org/10.1103/PhysRevLett.123.041102)
- Zhang, B. 2013, *ApJL*, 763, L22, doi: [10.1088/2041-8205/763/1/L22](https://doi.org/10.1088/2041-8205/763/1/L22)
- . 2018, *The Physics of Gamma-Ray Bursts*, doi: [10.1017/9781139226530](https://doi.org/10.1017/9781139226530)
- Zhang, B., & Mészáros, P. 2002, *ApJ*, 571, 876, doi: [10.1086/339981](https://doi.org/10.1086/339981)

- Zhang, B. B., Zhang, B., Sun, H., et al. 2018a, *Nature Communications*, 9, 447, doi: [10.1038/s41467-018-02847-3](https://doi.org/10.1038/s41467-018-02847-3)
- Zhang, D.-L., Li, X.-Q., Xiong, S.-L., et al. 2018b, arXiv e-prints, arXiv:1804.04499. <https://arxiv.org/abs/1804.04499>
- Zhu, J.-P., Wang, K., & Zhang, B. 2021a, *ApJL*, 917, L28, doi: [10.3847/2041-8213/ac1a17](https://doi.org/10.3847/2041-8213/ac1a17)
- Zhu, J.-P., Wang, K., Zhang, B., et al. 2021b, *ApJL*, 911, L19, doi: [10.3847/2041-8213/abf2c3](https://doi.org/10.3847/2041-8213/abf2c3)
- Zhu, J.-P., Wu, S., Yang, Y.-P., et al. 2021c, arXiv e-prints, arXiv:2106.15781. <https://arxiv.org/abs/2106.15781>
- Zhu, J.-P., Yang, Y.-P., Liu, L.-D., et al. 2020, *ApJ*, 897, 20, doi: [10.3847/1538-4357/ab93bf](https://doi.org/10.3847/1538-4357/ab93bf)
- Zhu, J.-P., Yang, Y.-P., Zhang, B., Gao, H., & Yu, Y.-W. 2021d, submitted to *ApJ*
- Zhu, J.-P., Zhang, B., Yu, Y.-W., & Gao, H. 2021e, *ApJL*, 906, L11, doi: [10.3847/2041-8213/abd412](https://doi.org/10.3847/2041-8213/abd412)
- Zhu, J.-P., Wu, S., Yang, Y.-P., et al. 2021f, *ApJ*, 917, 24, doi: [10.3847/1538-4357/abfe5e](https://doi.org/10.3847/1538-4357/abfe5e)